Free Radical Biology and Medicine 205 (2023) 244–261

Contents lists available at ScienceDirect

Free Radical Biology and Medicine

journal homepage: www.elsevier.com/locate/freeradbiomed

Energy substrate metabolism, mitochondrial structure and oxidative stress after cardiac ischemia-reperfusion in mice lacking UCP3

Patricia Sánchez-Pérez [a,b,1], Ana Mata [a,b,1], May-Kristin Torp [a,c], Elia López-Bernardo [a,b], Christina M. Heiestad [c], Jan Magnus Aronsen [c,d], Antonio Molina-Iracheta [e], Luis J. Jiménez-Borreguero [b,f,j], Pablo García-Roves [g,k,l], Ana S.H. Costa [h], Christian Frezza [h], Michael P. Murphy [i], Kåre-Olav Stenslokken [c], Susana Cadenas [a,b,*]

[a] Centro de Biología Molecular "Severo Ochoa" (CSIC/UAM), 28049, Madrid, Spain
[b] Instituto de Investigación Sanitaria Princesa (IIS-IP), 28006, Madrid, Spain
[c] Department of Molecular Medicine, Institute of Basic Medical Sciences, Faculty of Medicine, University of Oslo, PB1110, N-0317, Oslo, Norway
[d] Bjørknes College, 0456, Oslo, Norway
[e] Centro Nacional de Investigaciones Cardiovasculares Carlos III, 28029, Madrid, Spain
[f] Servicio de Cardiología, Hospital Universitario de La Princesa, 28006, Madrid, Spain
[g] Department of Physiological Sciences, Universitat de Barcelona, 08907, Barcelona, Spain
[h] MRC Cancer Unit, University of Cambridge, Hutchison/MRC Research Center, Cambridge Biomedical Campus, Cambridge, CB2 0XZ, UK
[i] MRC Mitochondrial Biology Unit, University of Cambridge, Wellcome Trust/MRC Building, Cambridge, CB2 0XY, UK
[j] Centro de Investigación Biomédica en Red Enfermedades Cardiovasculares (CIBERCV), Instituto de Salud Carlos III, 28029, Madrid, Spain
[k] Nutrition, Metabolism and Gene Therapy Group, Diabetes and Metabolism Program, Institut d'Investigació Biomèdica de Bellvitge (IDIBELL), Barcelona, Spain
[l] Centro de Investigación Biomédica en Red Fisiopatología de la Obesidad y la Nutrición (CIBEROBN), Instituto de Salud Carlos III, 28029, Madrid, Spain

ARTICLE INFO

Keywords:
Energy metabolism
Ischemia-reperfusion injury
Mitochondrial respiration
Mitochondrial structure
Oxidative stress
UCP3 (uncoupling protein 3)

ABSTRACT

Myocardial ischemia-reperfusion (IR) injury may result in cardiomyocyte dysfunction. Mitochondria play a critical role in cardiomyocyte recovery after IR injury. The mitochondrial uncoupling protein 3 (UCP3) has been proposed to reduce mitochondrial reactive oxygen species (ROS) production and to facilitate fatty acid oxidation. As both mechanisms might be protective following IR injury, we investigated functional, mitochondrial structural, and metabolic cardiac remodeling in wild-type mice and in mice lacking UCP3 (UCP3–KO) after IR. Results showed that infarct size in isolated perfused hearts subjected to IR *ex vivo* was larger in adult and old UCP3–KO mice than in equivalent wild-type mice, and was accompanied by higher levels of creatine kinase in the effluent and by more pronounced mitochondrial structural changes. The greater myocardial damage in UCP3–KO hearts was confirmed *in vivo* after coronary artery occlusion followed by reperfusion. S1QEL, a suppressor of superoxide generation from site I_Q in complex I, limited infarct size in UCP3–KO hearts, pointing to exacerbated superoxide production as a possible cause of the damage. Metabolomics analysis of isolated perfused hearts confirmed the reported accumulation of succinate, xanthine and hypoxanthine during ischemia, and a shift to anaerobic glucose utilization, which all recovered upon reoxygenation. The metabolic response to ischemia and IR was similar in UCP3–KO and wild-type hearts, being lipid and energy metabolism the most affected pathways. Fatty acid oxidation and complex I (but not complex II) activity were equally impaired after IR. Overall, our results indicate that UCP3 deficiency promotes enhanced superoxide generation and mitochondrial structural changes that increase the vulnerability of the myocardium to IR injury.

* Corresponding author. Centro de Biología Molecular "Severo Ochoa" (CSIC/UAM), C/ Nicolás Cabrera, 1, Cantoblanco, 28049, Madrid, Spain.
E-mail address: scadenas@cbm.csic.es (S. Cadenas).
[1] Equal contribution.

https://doi.org/10.1016/j.freeradbiomed.2023.05.014
Received 19 March 2023; Received in revised form 22 April 2023; Accepted 15 May 2023
Available online 8 June 2023

1. Introduction

Myocardial ischemia associated with acute coronary syndrome and acute myocardial infarction is a leading cause of morbidity and mortality. The lack of oxygen and nutrients during ischemia followed by blood flow restoration at reperfusion triggers ischemia-reperfusion (IR) injury, which occurs after reperfusion of a globally ischemic myocardium (cardiac arrest during cardiac surgery), or in the setting of regional IR. The underlying mechanisms include metabolic alterations, reactive oxygen species (ROS) overproduction, intracellular calcium overload, autophagy deregulation and mitochondrial dysfunction [1]. Mitochondrial dysfunction and a burst of ROS production are particularly relevant in the pathogenesis of IR injury [2–5]. Although there are several sources of superoxide and hydrogen peroxide in cardiomyocytes during IR, including NADPH oxidases, xanthine oxidase and uncoupled nitric oxide synthase, the mitochondrial electron transport chain is considered as the most important source of ROS [3,6]. Chouchani et al. reported that succinate-driven reverse electron transport (RET) leads to mitochondrial matrix superoxide production from complex I early in reperfusion [7,8]. In this context, inhibitors of the electron transport chain and chemical uncouplers such as 2,4-dinitrophenol (DNP) or FCCP have been demonstrated to reduce infarct size following IR injury in preclinical models of IR injury [9–13].

Uncoupling protein 3 (UCP3) is a member of the mitochondrial uncoupling protein family, and is abundantly expressed in tissues with a high capacity for fatty-acid β-oxidation (FAO), such as brown adipose tissue, skeletal muscle, and the heart. Unlike UCP1, the first UCP identified, the primary role of UCP3 is not adaptive thermogenesis. Mice lacking UCP3 are not obese, are normophagic and have normal overall energy expenditure [14,15]. The prevailing view is that UCP3 does not catalyse the basal proton conductance in skeletal muscle [16–19] or heart mitochondria [20]. Extensive experimental evidence suggests that UCP3 protects against excessive mitochondrial superoxide generation and oxidative stress [21–24]. Superoxide, or downstream lipid peroxidation products such as 4-hydroxy-2-nonenal, have been shown to activate UCPs, providing a feedback mechanism that depresses respiratory chain superoxide production by increasing proton leak across the inner mitochondrial membrane [25,26], although this has been questioned [27,28]. UCP3 expression is upregulated in mouse cardiomyocytes in response to oxidative stress to promote survival [29,30]. Moreover, UCP2 and UCP3 contain reactive cysteine residues that can be conjugated with glutathione, and this reversible modification regulates their function [31].

Beyond its role in protecting against excessive mitochondrial ROS production, UCP3 is reportedly involved in FAO, although its precise function is still unclear. The availability of fatty acids in skeletal muscle cells controls UCP3 gene expression *via* PPARα activation, suggesting that UCP3 gene expression contributes to the adaptive response to fatty acid catabolism [32]. Early studies proposed a function for UCP3 in exporting long-chain fatty acid (LCFA) anions from mitochondria [33]. In skeletal muscle, UCP3 induction limits mitochondrial ROS production by increasing the efficiency of FAO [34,35]. Using skeletal muscle mitochondria from mice lacking UCP3, Seifert et al. showed that this protein is not required for FAO, but is instead necessary for the fasting-induced enhancement of FAO rate and capacity, possibly by attenuating mitochondrial oxidative stress [36]. A later study reported that UCP3 deficiency in mice results in a metabolic shift in skeletal muscles that favors anaerobic glycolytic metabolism, increased glucose uptake, and enhanced sensitivity to oxidative challenge [37]. Additionally, association studies point to a role for UCP3 in insulin resistance [38,39].

Several studies have shown that UCP3 protects the heart against IR injury, and modulation of mitochondrial superoxide generation, apoptotic cell death, and energy metabolism are some of the proposed mechanisms [40–43]. Also, UCP3 induction by PPARα agonists was found to reduce infarct size after IR by limiting ROS generation [44]. In the present study, we explored the cardioprotective role of UCP3 in IR injury using isolated perfused hearts and transient coronary artery ligation in mice lacking UCP3 and wild-type mice. We also analyzed the impact of UCP3 deficiency on energy substrate metabolism, mitochondrial structure and oxidative stress.

2. Methods

1. *Animals.* Male UCP3 knockout (UCP3–KO) mice and wild-type C57BL/6J littermates were bred in the animal facility of the Centro de Biología Molecular "Severo Ochoa" (CSIC/UAM; Madrid, Spain), and were maintained on a normal rodent diet with *ad libitum* access to food and water. Experiments were performed in adult (20–22 weeks old) or old (78–80 weeks old) male mice. Body weight (g) was similar in wild-type and UCP3–KO adult mice (31.5 ± 1.08 vs 31.8 ± 0.95; n = 8) as previously reported for both adult and old mice [14,15,19]. All procedures were performed in accordance with the guidelines and regulations of the Centro de Biología Molecular "Severo Ochoa" (Madrid, Spain; PROEX 146/15, 120.2/21), Centro Nacional de Investigaciones Cardiovasculares (CNIC; Madrid, Spain; PROEX 332/15), and the University of Oslo (Oslo, Norway; FOTS 12211).
2. *Langendorff perfusion of isolated hearts.* Mice were killed by cervical dislocation and the hearts were immediately excised and rinsed in ice-cold Krebs-Henseleit buffer (KHB), consisting of 120 mM NaCl, 25 mM $NaHCO_3$, 11 mM glucose, 1.2 mM KH_2PO_4, 1.2 mM $MgSO_4$, 4.8 mM KCl, and 2 mM $CaCl_2$. Heart weight (mg) was similar in wild-type and UCP3–KO adult mice (164 ± 8.60 vs 161 ± 6.88; n = 8) as previously reported [15,45]. Hearts were cannulated via the aorta (0.8 mm diameter cannula) and perfused retrogradely with warm (37 °C) oxygenated KHB on a Langendorff apparatus. The heart was immersed at all times in perfusion solution that was maintained at 37 °C via water jackets. The solution was bubbled with a gas mixture of 95% O_2/5% CO_2 to maintain pH 7.4. Aortic pressure was monitored continuously using a pressure transducer (Transpac IV, ICU Medical, Inc., CA) located above the cannula. The flow rate was kept constant at 2 mL/min using a peristaltic pump (ISMATEC International, Wertheim, Germany) that maintained the pressure of approximately 70–80 mmHg. Recordings were obtained using a PowerLab 2/20 system (ADInstruments, Oxfordshire, UK) and PowerLab Chart software v5.4.2 (ADInstruments).

Mouse hearts were perfused following different protocols: 1) control (C): hearts were perfused with standard oxygenated KHB at 37 °C for 120 min; 2) ischemia (I): hearts were allowed to stabilize for 20 min before the flow was completely stopped to generate global normothermic ischemia for 40 min; 3) ischemia-reperfusion (IR): hearts were allowed to stabilize for 20 min before generating global normothermic ischemia for 40 min followed by reperfusion for 60 min; 4) ischemic preconditioning (IPC): hearts were allowed to stabilize for 20 min before applying 2 cycles of 5-min ischemia plus 5-min reperfusion, and they were then subjected to global normothermic ischemia for 40 min followed by 60 min of reperfusion. In some experiments, the small-molecule suppressor of site I_Q electron leak S1QEL1.1 (cat# 20982; Cayman Chemical Co., Ann Arbor, MI) was perfused at 1 μM in KHB for 5 min at the beginning of reperfusion. In these experiments, mice were anesthetized with an i.p. injection of xylazine (10 mg/kg) and ketamine (100 mg/kg) containing heparin (500 IU/mL), and the control IR hearts were perfused with KHB containing 0.50 μL/mL (v/v) of DMSO.

3. *Infarct size measurement.* Upon completion of the experimental perfusion protocol, perfused hearts were stained with triphenyltetrazolium chloride (TTC; Sigma-Aldrich, Madrid, Spain) to determine infarct size. TTC (1% in PBS) was perfused through the cannula at 1 mL/min for 12 min at 37 °C. The heart was then removed from the cannula, immersed in PBS, and kept at 37 °C for 5 min.

Subsequently, the heart was sectioned into 4–5 slices about 2 mm thick, which were then fixed overnight in 4% formaldehyde, washed with water, photographed on both sides, allowed to dry for 24 h over desiccant paper, and weighted. Images were analyzed for infarct size using AlphaEaseFC software (Alpha Innotech, San Leandro, CA). The percentage of infarcted volume of the whole heart was calculated considering the images from both sides of each slide, and the contribution of each particular slice to the total dried weight of the heart.

4. *Creatine kinase activity.* Creatine kinase (CK) activity in the coronary effluent was measured to determine IR injury. Aliquots of coronary effluent were collected prior to ischemia for basal levels, and during reperfusion. The samples were maintained at 4 °C and analyzed for CK activity on the same day of the experiment using the CK-NAC kit (CK113, Randox, Belfast, UK). Total CK activity was calculated as the area under the curve (AUC).
5. *Left anterior descending coronary artery ligation and reperfusion.* Mice were first anesthetized (i.p.) with pentobarbital sodium (50 mg/kg), and then intubated and ventilated on a small rodent ventilator (Harvard Apparatus, Holliston, MA). Open-chest left anterior descending (LAD) coronary artery ligation was used to induce IR injury. The left coronary artery was ligated with a 8-0 nylon suture, and the heart was subjected to 45 min of ischemia. The ligation was then released to reperfuse the myocardium. The core temperature was maintained at 37 °C with a heating pad. Analgesia was supplied in the drinking water after surgery. All experiments were terminated at day 21 post-operation, when the animals were killed by cervical dislocation and the hearts were processed for histology.
6. *Echocardiography.* Transthoracic echocardiography was performed to evaluate heart function after *in vivo* IR. Measurements were taken 3 days before surgery, and at 3 and 21 days after surgery (45-MHz probe; VisualSonics Vevo 770, Toronto, Canada). Animals were analyzed under light inhaled anesthesia (1.5% isoflurane at 0.8–1.0 L/min). Mice were placed supine on a heating platform at 37 °C. Body temperature was monitored using a rectal temperature probe, and cardiac function was continuously monitored by echocardiography. Two-dimensional (2D) echocardiography images were acquired in the long axis view and in the short axis at mid and apical levels of the left ventricle (LV). Using the area-length method, LV end-systolic volume (LVESV), end-diastolic volume (LVEDV), and LV ejection fraction (EF) [((LVEDV-LVESV)/LVEDV) × 100], were measured to detect global LV functional impact of the myocardial infarction [46]. For a precise echocardiographic analysis of the functional impact of the infarct size, regional LV motion was evaluated by a score [46]. Briefly, the LV wall was divided into 13 segments (basal, mid and apical from the anterior, posterior, lateral and septal walls, as well as the apex). Each segment was scored in a blind manner based on motion and systolic thickening, according to the American Society of Echocardiography guidelines (1, normal or hyperkinetic; 2, hypokinetic; 3, akinetic, negligible thickening; dyskinetic, paradoxical systolic motion; 5, aneurysmal, diastolic deformation) [47]. The number of dysfunctional segments was quantified, and the total score representing the sum of the score of the 13 individual segments was calculated for each heart. Pulsed Doppler of mitral flow was recorded to assess impaired E:A wave as indirect impact of the myocardial infarction in the LV diastolic function. All images were analyzed using the Vevo LAB (VisualSonics) ultrasound analysis software.
7. *Histological analysis.* Hearts were fixed in 10% neutral buffered formalin (Sigma-Aldrich) for 48 h. Three sections were used at three different levels from the apex to the base of the heart and were processed by dehydrating the tissue in a graded ethanol series. Tissues were then cleared in xylene, embedded in paraffin wax, and sectioned at a thickness of 4 μm. For histopathological evaluation, sections were stained with hematoxylin and eosin (H&E) and Masson's trichrome stain. For image analysis, the samples were digitized with a scanner (Nanozoomer-RS C110730®; Hamamatsu, Japan). The total area of the heart section was quantified on the digital files using image analysis software (Tissuemorph®; Visiopharm A/S Hoersholm, Denmark). The area of infarcted tissue was manually quantified on the same digital files and the percentage of lesion to total area was calculated.
8. *Transmission electron microscopy analysis of cardiac mitochondrial ultrastructure.* Immediately after completion of the perfusion protocol, heart pieces of ~1 mm^3 of the left ventricular area near the apex were fixed with 4% paraformaldehyde and 2% glutaraldehyde in 0.1 M phosphate buffer (pH 7.4) for 2 h at room temperature and then overnight at 4 °C. Subsequently, a post-fixation step with 1% osmium tetroxide and 0.8% potassium ferricyanide was performed for 1 h at 4 °C. Following the post-fixation, the samples were incubated with 0.15% tanic acid for 1 min at room temperature and subsequently incubated with 2% uranyl acetate for 1 h at room temperature in the dark. Samples underwent a solvent-based dehydration step followed by embedding in TAAB 812 epoxy resin (TAAB Laboratories, Berkshire, UK), prior to ultra-fine sectioning and post-staining with a heavy metal stain. Ultra-fine sections of 70 nm were cut with an Ultracut E ultramicrotome (Leica Systems, Wetzlar, Germany) and mounted on Formvar-carbon-coated Cu/Pd slot grids. The heavy metal staining was performed with uranyl acetate and lead citrate. A JEM-1400 Flash electron microscope (JEOL Ltd., Tokyo, Japan) was used at 100 kV to visualize the samples, and a OneView 4 k × 4 k CMOS camera (Gatan, Pleasanton, CA) was used to acquire images.

Mitochondrial morphology was analyzed in 100 mitochondria per sample in randomly selected micrographs (6000 × magnification). Mitochondria were classified into four classes according to their ultrastructure [48]: class I: mitochondria present numerous narrow pleomorphic cristae, appearing in transmission electron microscopy (TEM) as small electron-transparent areas, in a contiguous electron-dense matrix space; class II: mitochondria are in a remodeled state characterized by a serpentine electron-transparent intracristal compartment interrupted by electron-dense matrix spaces; the cristae and matrix spaces are markedly reorganized; class III: mitochondria have progressed to gross morphological derangement, with asymmetric blebbing of herniated matrix resulting in a partial rupture of the outer membrane and swelling on one side of the mitochondrion; class IV: terminally swollen and ruptured mitochondria with little or no distinguishable cristae structure. The number of inter-mitochondrial junctions [49] were counted in 100 mitochondrial contacts per sample in randomly selected micrographs (6000 × magnification). The number of lipid droplets per unit area was counted in randomly selected micrographs (6000 × magnification) and expressed as lipid droplets per mm^2.

9. *Metabolomics analysis.* Immediately after *ex vivo* perfusion of the hearts, tissues were weighed and frozen in liquid nitrogen and stored at −80 °C. Tissues were homogenized using glass homogenizers at 4 °C followed by hydrophilic extraction of intracellular metabolites. We used 250 μL of cold extraction solution (50% methanol, 30% acetonitrile and 20% water, plus 100 ng/mL HEPES) per 10 mg of homogenized tissue. Samples were then vortex-mixed for 2 min and centrifuged at 16,000 *g* at 4 °C for 10 min. The supernatants containing the metabolite extracts were maintained at −80 °C, coded and shipped on dry ice from the CBMSO (Madrid) to the MRC Cancer Unit (University of Cambridge) for blinded metabolomic analysis. Metabolites were analyzed by liquid chromatography coupled to mass spectrometry (LC-MS).
10. *Respiration measurements of heart biopsies.* Mitochondrial respiration was determined by high-resolution respirometry (Oxygraph-2k; Oroboros Instruments, Innsbruck, Austria). Upon completion of perfusion, a sample of the LV (~10 mg) was weighed and immediately homogenized using a PBI Shredder homogenizer

(Oroboros Instruments) in mitochondrial respiration medium (MiR05, Oroboros Instruments) containing 0.5 mM EGTA, 3 mM $MgCl_2$, 60 mM lactobionic acid, 20 mM taurine, 10 mM KH_2PO_4, 20 mM HEPES, 110 mM D-sucrose and 1 g/L fatty acid-free BSA at 4 °C. Oxygen consumption was determined in homogenates (2 mL) gently agitated at 37 °C in parallel Oxygraph-2k chambers, at a concentration of 0.75 mg/mL in MiR05. At air saturation, 37 °C, and local barometric pressure (93.3 kPa), the oxygen concentration in MiR05 was 177.1 μM (O_2 solubility factor 0.92). Initial oxygen levels were increased to 400 μM by perfusion of oxygen into the chambers, and the medium was reoxygenated when the oxygen concentration fell below 230 μM. The instrumental background flux was calculated as a linear function of oxygen concentration and experimental data were corrected for the whole range of oxygen concentration using DatLab software (Oroboros Instruments). Oxygen consumption was determined following sequential additions of ADP (5 mM), $MgCl_2$ (3 mM), malate (0.5 mM), octanoylcarnitine (750 μM), pyruvate/malate (5 mM/2 mM), glutamate (10 mM), succinate (10 mM) and glycerophosphate (10 mM). Maximal respiration was determined after the addition of the uncoupler FCCP (1 μM). Rotenone (0.5 μM) was used to inhibit complex I. Non-mitochondrial respiration was determined after the addition of antimycin A (2.5 μM) to inhibit complex III and the value was subtracted from all other values.

11. *Measurement of H_2O_2 in isolated perfused hearts using MitoB.* Mice were anesthetized with an i.p. injection of xylazine (10 mg/kg) and ketamine (100 mg/kg) containing heparin (500 IU/mL). Isolated hearts were perfused with modified KHB [116 mM NaCl, 4.7 mM KCl, 1.2 mM $MgSO_4{\cdot}7H_2O$, 25 mM $NaHCO_3$, 11 mM glucose, and 1.4 $CaCl_2$, continuously gassed with 95% O_2/5% CO_2 (pH 7.4, 37 °C)] and subjected to 40 min of ischemia followed by 15 min of reperfusion. MitoB (10 μM) was perfused in a recirculating Langendorff system throughout the experiment at a constant pressure of 70 mmHg. MitoB concentrates in the mitochondrial matrix where it is converted to MitoP by reacting with H_2O_2. Upon completion of the perfusion protocol, hearts were snap-frozen in liquid N_2 and weighed to approximately 50 mg for LC-MS analysis. Samples were shipped on dry ice from the University of Oslo to the MRC Mitochondrial Biology Unit in Cambridge for processing and analysis. Samples were processed using the standard MitoB and MitoP extraction method [8], adapted for extraction using a Precellys® tissue homogenizer (Bertin Instruments, Paris, France). Standard curves were processed in conjunction with the sample set, with untreated tissue sent from the University of Oslo. Each sample was spiked with 10 μL of a stock master mix of internal standard (10 μM MitoB-d_{15}/5 μM MitoP-d_{15}) to determine extraction and quantification efficiency. The ratio MitoP/MitoB, the indicator of H_2O_2 levels, was determined by LC-MS/MS analysis using a Waters Xevo TQ-S mass spectrometer (Waters, Manchester, UK). Separation was achieved using an Acquity UPLC BEH 1.7 μm C18 column (Waters). Spectra data were processed using MassLynx software (Waters), and all data were acquired based on MS response relevant to the internal standards.
12. *Isolation of adult mouse cardiomyocytes.* Adult mouse cardiomyocytes were isolated after retrograde perfusion of collagenase through the coronary arteries [50]. Briefly, the hearts were immediately dissected and perfused with perfusion buffer [120.4 mM NaCl, 14.7 mM KCl, 0.6 mM KH_2PO_4, 0.6 mM Na_2H-$PO_4{\cdot}2H_2O$, 1.2 mM $MgSO_4{\cdot}7H_2O$, 10 mM Na-HEPES, 4.6 mM $NaHCO_3$, 30 mM taurine, 10 mM 2,3-butanedione monoxime (BDM), 5.5 mM glucose·$1H_2O$, pH 7.0] for 4 min at 4 mL/min. A digestion buffer containing 1.3 mg/mL Collagenase Type II (cat# LS004176, batch 47K17724B, 270 U/mg, Worthington Biochemical, Lakewood, NJ) was then perfused for 11 min at a flux of 4.0 mL/min to promote extracellular matrix degradation, in the presence of 40 μM $CaCl_2$ for the last 8 min. After collagenase perfusion, the heart was finely cut with sharp scissors and re-suspended in 5 mL perfusion buffer. Cardiomyocytes were then gradually introduced to increasing calcium concentrations from 12.5 to 900 μM $CaCl_2$. Cardiomyocytes were cultured in laminin-coated plates with MEM with Hanks BSS medium (Sigma-Aldrich, ref. M5775) supplemented with 10% calf serum, 2 mM glutamine, 10 mM BDM, 100 U/mL penicillin and 100 μg/mL streptomycin at 37 °C and 5% CO_2 for 1–2 h. The medium was subsequently changed to MEM with Hanks BSS medium supplemented with 0.10% fatty acid-free BSA, 2 mM glutamine, 1 mM BDM, 100 U/mL penicillin and 100 μg/mL streptomycin. Cardiomyocytes were first subjected to 0.5% O_2 (hypoxia) and 5% CO_2 at 37 °C for 40 min and then reoxygenated for 2 h before viability and LDH release assays (see below).
13. *Viability assay of isolated cardiomyocytes.* Cardiomyocyte viability was measured in cells cultured in Lab-Tek II 8-well glass chamber slides (Thermo Fisher Scientific Inc., Waltham, MA), and stained with 1 μM Hoechst 33258 (Thermo Fisher Scientific Inc.), 16.6 nM MitoTracker® Deep Red FM (Thermo Fisher Scientific Inc.), and 12.5 μM propidium iodide solution for 30 min at 37 °C in 2% CO_2. After incubation, the cells were washed twice in PBS and fixed for 10 min at 37 °C in 2% CO_2 with 2% paraformaldehyde in PBS. Gelatine-glycerol mounting medium, pre-heated to 55 °C was added to the slides, which were then sealed with a cover glass. The slides were analyzed with a Zeiss high-throughput microscope (Carl Zeiss AG, Oberkochen, Germany) at 10 × magnification. Twenty-five images were automatically captured per well and Hoechst-stained nuclei served for image-based autofocus. Cardiomyocytes (MitoTracker-stained) were counted and propidium iodide-stained nuclei (indicator of cell death) were counted within nuclei of MitoTracker-stained cardiomyocytes with Cell profiler™ cell image analysis software [51]. Results are either presented as a ratio of total number of propidium iodide-stained nuclei and total number of nuclei (ratio cell death), or as eccentricity of cardiomyocytes in order to evaluate cardiomyocyte morphology as unhealthy/dead (circular) or healthy/intact (rod shaped) cardiomyocytes.
14. *Lactate dehydrogenase activity.* LDH was determined in the culture medium of isolated adult cardiomyocytes after hypoxia/reoxygenation (H/R). The samples were maintained at 4 °C and analyzed for LDH activity on the same day of the experiment using the Cytotoxicity Detection Kit (LDH) (Roche, Basel, Switzerland).
15. *Statistical analysis.* The data are presented as the mean ± SEM. The statistical significance of the differences between means was calculated using two-tailed Student's *t*-test for pairwise comparisons or two-way ANOVA followed by Tukey's *post-hoc* test for multiple comparisons using GraphPad Prism software. A P value of <0.05 was considered statistically significant.

3. Results

3.1. Lack of UCP3 increases infarct size and creatine kinase activity in adult and old ex vivo hearts following IR

We evaluated infarct size (TTC staining) in isolated perfused hearts from UCP3–KO and wild-type mice subjected to IR to confirm previous reports on the cardioprotective role of UCP3 in IR injury (Fig. 1A). Since the aged heart is more susceptible to injury after IR [52,53], both adult (20–22 weeks) and old (78–80 weeks) mice were used. As shown in Fig. 1B and C, the infarct size calculated as the percentage of the infarct area divided by the total area, was significantly greater in adult hearts lacking UCP3 than in equivalent wild-type hearts. The infarct size tended to be greater in UCP3–KO hearts from old mice. These results

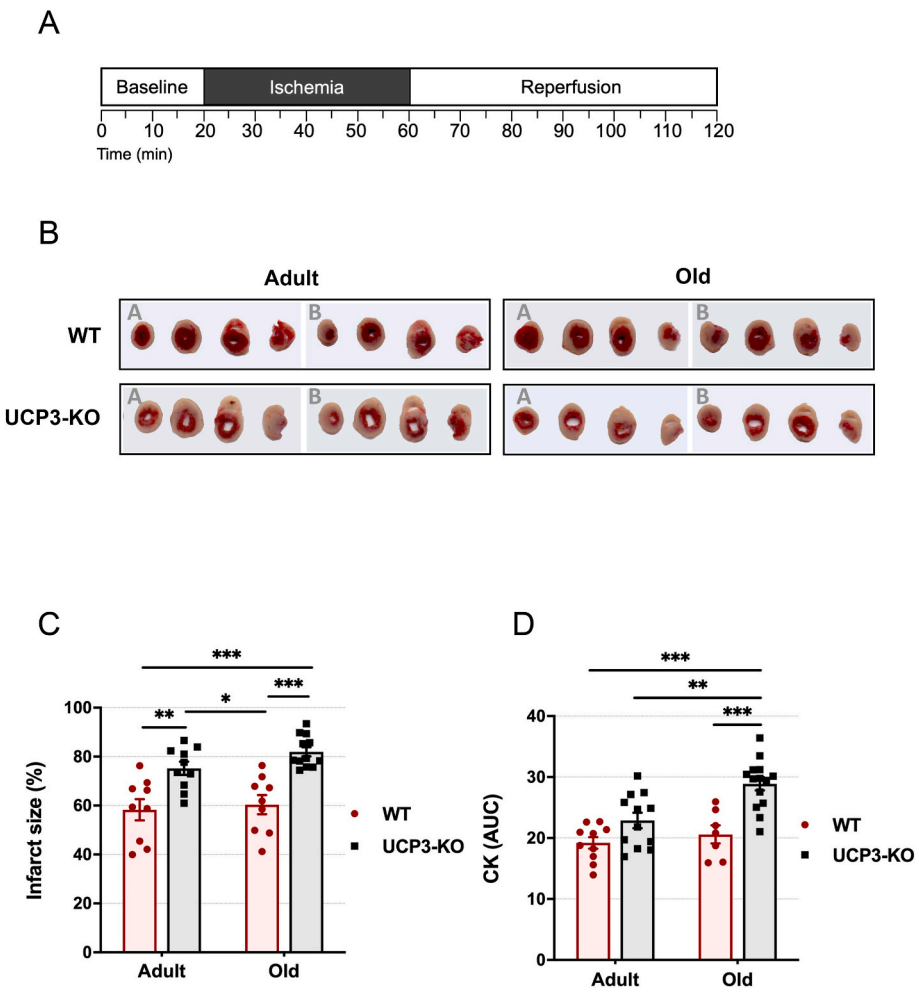

Fig. 1. Infarct size and creatine kinase activity in isolated perfused hearts from adult and old wild-type and UCP3–KO mice after ischemia-reperfusion. (A) Langendorff perfusion protocol. (B) Representative images of heart slices from adult (20–22 weeks) and old (78–80 weeks) wild-type and UCP3–KO mice subjected to ischemia-reperfusion (IR) and stained with tetrazolium chloride (TTC). The viable zone was stained in red, whereas the infarcted area remained white. (C) Histograms show the mean ± SEM of the percentage of infarct as the necrotic area (white) related to the total area, from 9 to 11 hearts per group. (D) Enzymatic analysis of creatine kinase (CK) measured in the coronary effluent over time during reperfusion. Histograms show the mean ± SEM of the area under the curve (AUC) from 7 to 12 hearts per group. $^{*}P < 0.05$, $^{**}P < 0.01$, $^{***}P < 0.001$.

indicate that UCP3 plays a cardioprotective role against IR injury that could be more relevant in old than in adult mice.

We also measured CK activity in the coronary effluent during reperfusion. CK is released from the cytosol of damaged cells to systemic circulation and is a sensitive marker of myocardial infarction. Basal CK levels were determined after stabilization and just prior to ischemia, while reperfusion levels were determined throughout the 60-min reperfusion period. CK activity (AUC) in the effluent was higher in UCP3–KO hearts than in wild-type hearts, and was higher in UCP3–KO hearts from old mice than from adult mice (Fig. 1D). These results mirrored the data for infarct size, and confirm that IR elicits greater damage in isolated perfused hearts from mice lacking UCP3 than from wild-type mice. The data also confirm a protective role for UCP3 in cardiac IR injury and indicate that aged hearts from UCP3–KO mice are more susceptible to IR injury.

3.2. Lack of UCP3 increases infarct size following LAD coronary artery ligation, but does not aggravate left ventricular dysfunction

To test whether UCP3 also protects the heart *in vivo* against IR injury, we performed LAD coronary artery ligation (45 min) followed by reperfusion in adult UCP3–KO and wild-type mice (Fig. 2A). Tissue damage was determined by histology (Fig. 2B, S1), and its functional impact was assessed by measuring global and regional systolic LV function was well as diastolic function by echocardiography (Table 1). Analysis showed that LV EF decreased similarly in both types of hearts after LAD ligation. LV contractility regional score and LV volumes were only slightly higher in UCP3–KO mice than in wild-type mice following LAD ligation. E:A elevation reflects diastolic dysfunction following IR.

Once the echocardiography at 21 days post-surgery was performed, the hearts were processed for histological analysis. 21 days after coronary artery ligation, there was still significant remodeling with infiltration of leukocytes and inflammatory response, and little thinning of the left ventricular wall. Results showed that the infarct area was significantly larger in UCP3–KO mice than in wild-type mice (Fig. 2B and C, S1), thus confirming the cardioprotective role of UCP3 in IR injury *in vivo*.

3.3. S1QEL limits the infarct size in isolated perfused hearts from UCP3–KO mice after IR

Given that UCP3 protects against cardiac IR injury both *ex vivo* and *in vivo*, and considering its likely role in the control of mitochondrial ROS production, we reasoned that the greater damage in UCP3–KO hearts was because of enhanced ROS production at reperfusion. We thus used the MitoB radiometric probe to study the level of H_2O_2 15 min after reperfusion in isolated perfused UCP3–KO and wild-type hearts subjected to IR (Fig. S2A). However, the MitoP/B ratio indicated that the level of mitochondrial H_2O_2 in UCP3–KO and wild-type hearts was similar (Fig. S2B).

Although the levels of H_2O_2 were similar in both groups at 15 min reperfusion, we hypothesized that UCP3–KO hearts might generate more superoxide than wild-type hearts earlier during reperfusion. Superoxide is generated in complex I during reperfusion. We therefore perfused the

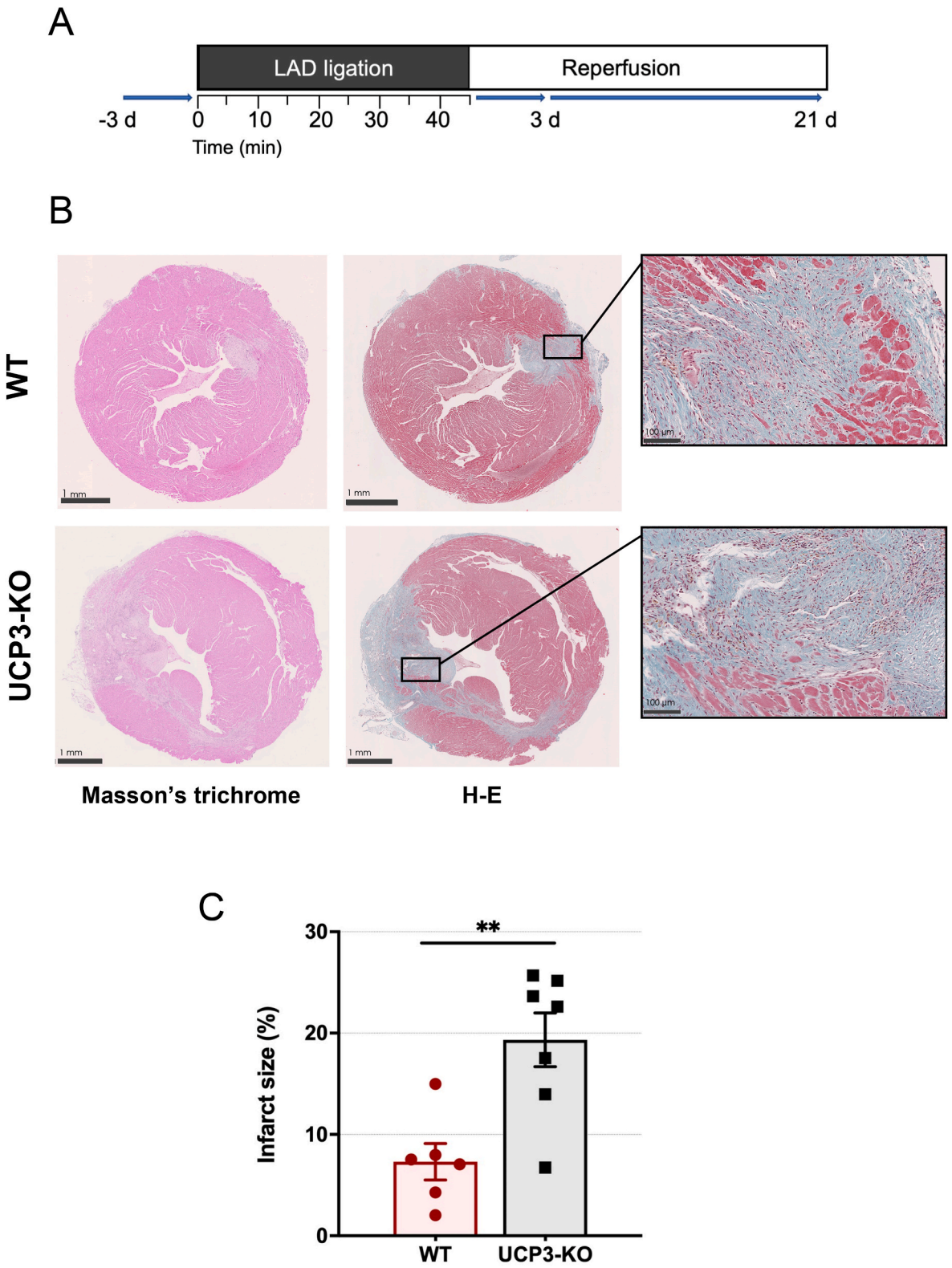

Fig. 2. *In vivo* myocardial infarction following coronary artery ligation in adult wild-type and UCP3–KO mice. (A) Mice were subjected to left anterior descending (LAD) coronary artery ligation for 45 min followed by reperfusion, and were sacrificed 21 days after surgery. (B) Histological analysis of heart sections with hematoxylin and eosin or Masson's trichrome stain (2 × magnification; scale bar 1,00 mm). Magnified fibrotic areas are shown in the insets (20 × magnification; scale bar 100 µm). (C) Histograms show the mean ± SEM of the percentage of infarct area relative to total area from 6 to 7 hearts per group. $^{**}P < 0.01$.

Table 1
Echocardiography analysis of UCP3–KO and wild-type mice following LAD coronary artery ligation. The table shows the means ± SEM of the parameters analyzed from 9 to 10 mice per group. The mortality rate was similar in both groups of mice (~30%). MI, myocardial infarction; LV EF, left ventricular ejection fraction; LVESV, left ventricular end-systolic volume; LVEDV, left ventricular end-diastolic volume; E:A, E:A ratio (mitral flow).

LAD ligation (45 min)	3 days pre-MI		3 days post-MI		21 days post-MI	
	WT	UCP3–KO	WT	UCP3–KO	WT	UCP3–KO
LV EF (%)	50.8 ± 2.2	49.0 ± 3.7	29.4 ± 2.6	29.7 ± 4.2	27.3 ± 3.0	31.5 ± 4.6
LVEDV (μL)	61.7 ± 7.2	68.6 ± 7.5	54.3 ± 3.3	58.8 ± 2.2	67.6 ± 5.3	81.8 ± 7.4
LVESV (μL)	34.5 ± 3.1	36.4 ± 6.8	38.0 ± 2.5	37.7 ± 4.2	49.4 ± 5.0	57.2 ± 8.1
E:A	1.26 ± 0.1	1.21 ± 0.1	2.12 ± 0.3	2.03 ± 0.4	1.61 ± 0.1	1.58 ± 0.1
Score	–	–	3.7 ± 0.57	4.3 ± 0.87	4.0 ± 0.72	4.6 ± 0.88

compound S1QEL (suppressor of site I_Q electron leak) for 5 min at the time of reperfusion (Fig. 3A), and then determined infarct size under these conditions. We found a trend for a reduction in infarct size in S1QEL-treated UCP3–KO hearts, albeit not significant (Fig. 3B and C), suggesting the excessive production of mitochondrial superoxide from site I_Q in UCP3–KO hearts as compared with wild-type hearts. These results were confirmed by analyzing CK activity (Fig. 3D).

3.4. IR induces changes in cardiac mitochondrial morphology and organization

To study the structural changes in mitochondrial shape and organization after IR, we analyzed TEM images of isolated perfused hearts. As shown in Fig. 4A, *ex vivo* IR induced evident changes in mitochondrial morphology and ultrastructure, and these changes were more pronounced in UCP3–KO hearts than in wild-type hearts. In particular, the cristae and matrix spaces appeared reorganized (class II), and exhibited gross morphological derangement (class III), leading to fragmentation (fission), swelling and, ultimately, rupture of the outer membrane (class IV) (Fig. 4B). IR resulted in a lower number of mitochondrial junctions (Fig. 4C) and an accumulation of lipid droplets (Fig. 4D). Of note, UCP3–KO control mitochondria also showed enhanced remodeling, a reduced number of mitochondrial junctions and a higher accumulation of lipid droplets, which may reflect an impairment in FAO.

3.5. Lipid and energy metabolism are the most affected pathways after IR in UCP3–KO and wild-type hearts

To study the impact of IR on overall metabolism, and the potential role of UCP3 in this process, we performed a metabolomics analysis of isolated perfused hearts from UCP3–KO and wild-type mice subjected to ischemia or to IR (Fig. 5A). Because UCP3 has been involved in the protective phenomenon of IPC [41], we also included a preconditioned group of UCP3–KO and wild-type hearts (Fig. 5A). A supervised heat map of the analysis is shown in Fig. S3. Hearts from UCP3–KO and wild-type mice showed an overall similar metabolic response to ischemia (Fig. 5B–G): xanthine, hypoxanthine, succinate and lactate accumulated under ischemic conditions whereas glucose dramatically decreased. Both the decrease in glucose and the accumulation of lactate

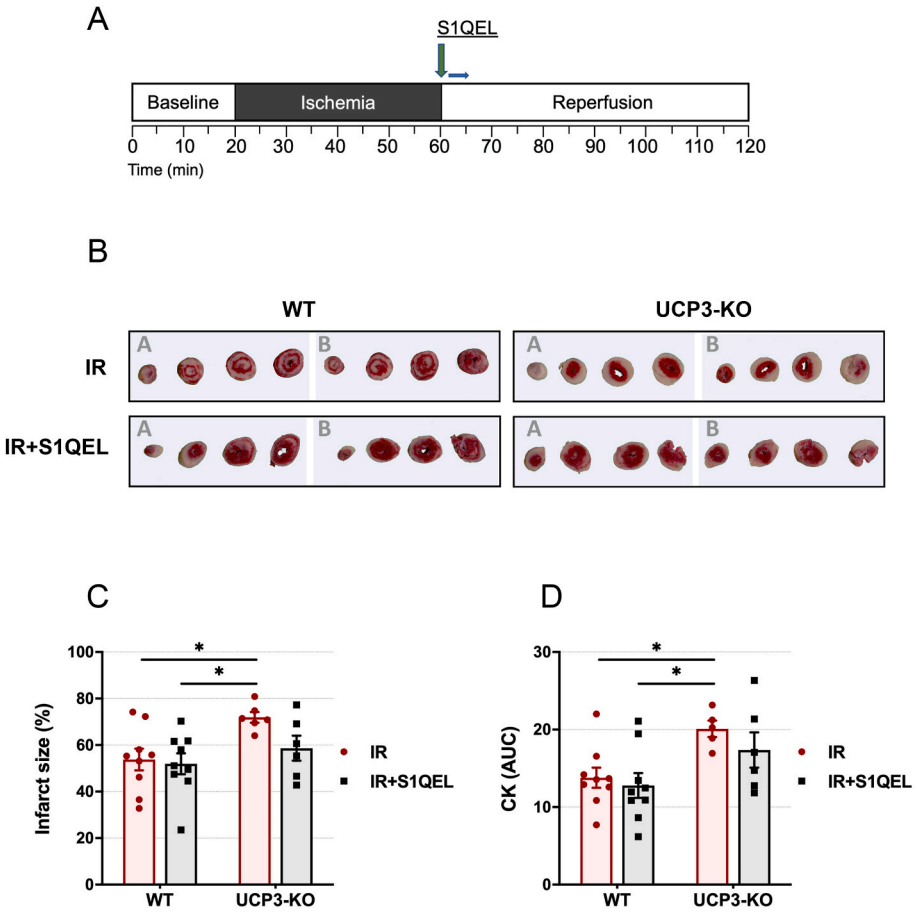

Fig. 3. Effect of S1QEL on infarct size and creatine kinase activity in isolated perfused hearts from adult wild-type and UCP3–KO mice following ischemia-reperfusion. (A) Langendorff perfusion protocol. S1QEL (S; 1 μM) was perfused in KHB for 5 min at the beginning of reperfusion. (B) Representative images of heart slices from wild-type and UCP3–KO mice perfused with S1QEL before ischemia-reperfusion (IR) and stained with tetrazolium chloride (TTC). (C) Histograms show the mean ± SEM of the percentage of infarct as necrotic area related to the total area, from 6 to 9 hearts per group. (D) Enzymatic analysis of creatine kinase (CK) measured in the coronary effluent over time during reperfusion. Histograms show the mean ± SEM of the area under the curve (AUC) from 6 to 9 hearts per group. *$P <$ 0.05.

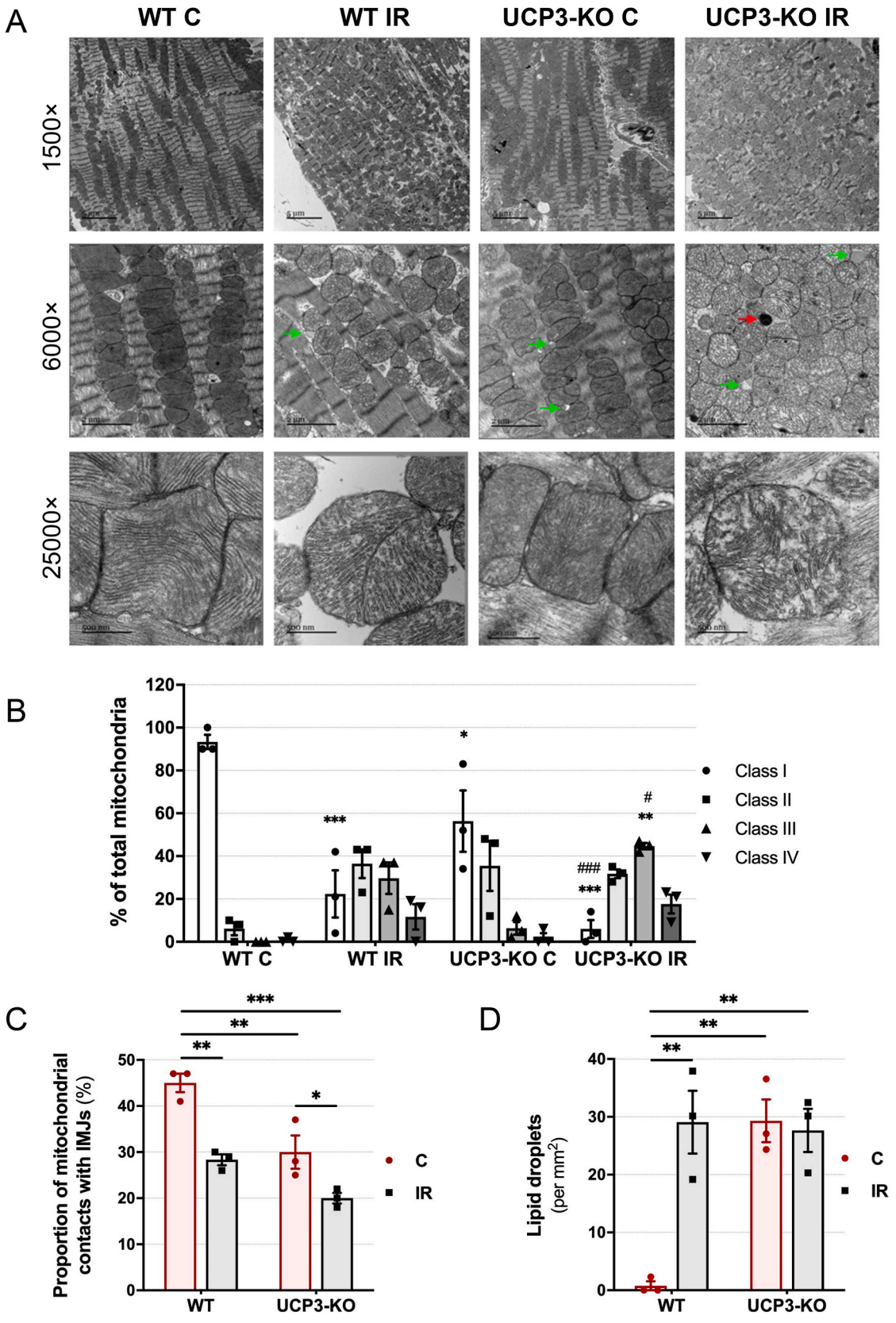

Fig. 4. Characterization of mitochondrial morphology by transmission electron microscopy. (A) Representative electron micrographs of hearts from adult wild-type and UCP3–KO mice after *ex vivo* ischemia-reperfusion (IR). Green arrows indicate lipid droplets; red arrows indicate electro-dense mitochondria. (B) Histograms show the mean ± SEM of the percentage of class class I–IV mitochondria from 3 sets of 100 mitochondria per group. $^{*}P < 0.05$, $^{**}P < 0.01$, $^{***}P < 0.001$ with respect to wild-type control of the same class; $^{\#}P < 0.05$, $^{\#\#\#}P < 0.001$ with respect to UCP3–KO control of the same class. (C) Histograms show the mean ± SEM of the number of inter-mitochondrial junctions from 3 sets of 100 mitochondria per group. $^{*}P < 0.05$. C, control; IR, ischemia-reperfusion.

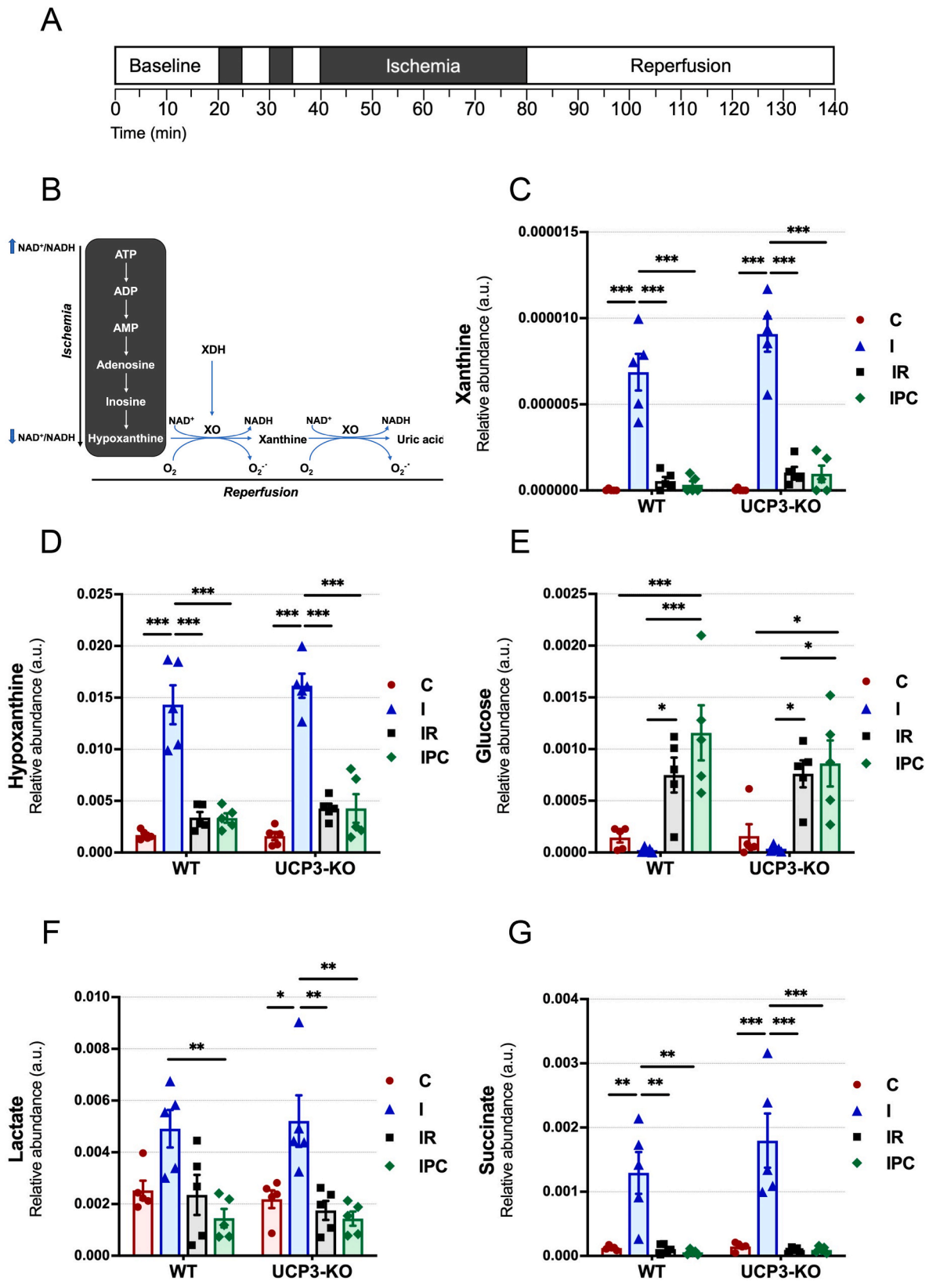

Fig. 5. Metabolite levels in isolated perfused hearts from adult wild-type and UCP3–KO mice subjected to different perfusion protocols. (A) Langendorff perfusion protocol. (B) Xanthine oxidase reaction and superoxide generation during reperfusion. Metabolic markers of stress-induced myocardial ischemia (C–F): xanthine, hypoxanthine, glucose and lactate; Krebs cycle intermediates (G–J): succinate, fumarate, malate and α-ketoglutarate; 2-hydroxyglutarate (K); ribose/ribulose-5-phosphate (L); alanine/glutamate (M); acylcarnitines (N−Q): isovalerylcarnitine, octanoylcarnitine, butyrylcarnitine and propionylcarntine; glycerol (R); fatty acids (S–W): oleic acid (18:1 n-9), stearic acid (18:0), palmitic acid (16:0), palmitoleic acid (16:1 n-7), linoleic acid (18:2 n-6) and orotic acid (X). Histograms show the mean ± SEM of the relative abundance (a.u.) from 5 mice per group. Abbreviations: C, control; I, ischemia; IR, ischemia-reperfusion; IPC, ischemic preconditioning. $^{*}P < 0.05$, $^{**}P < 0.01$, $^{***}P < 0.001$.

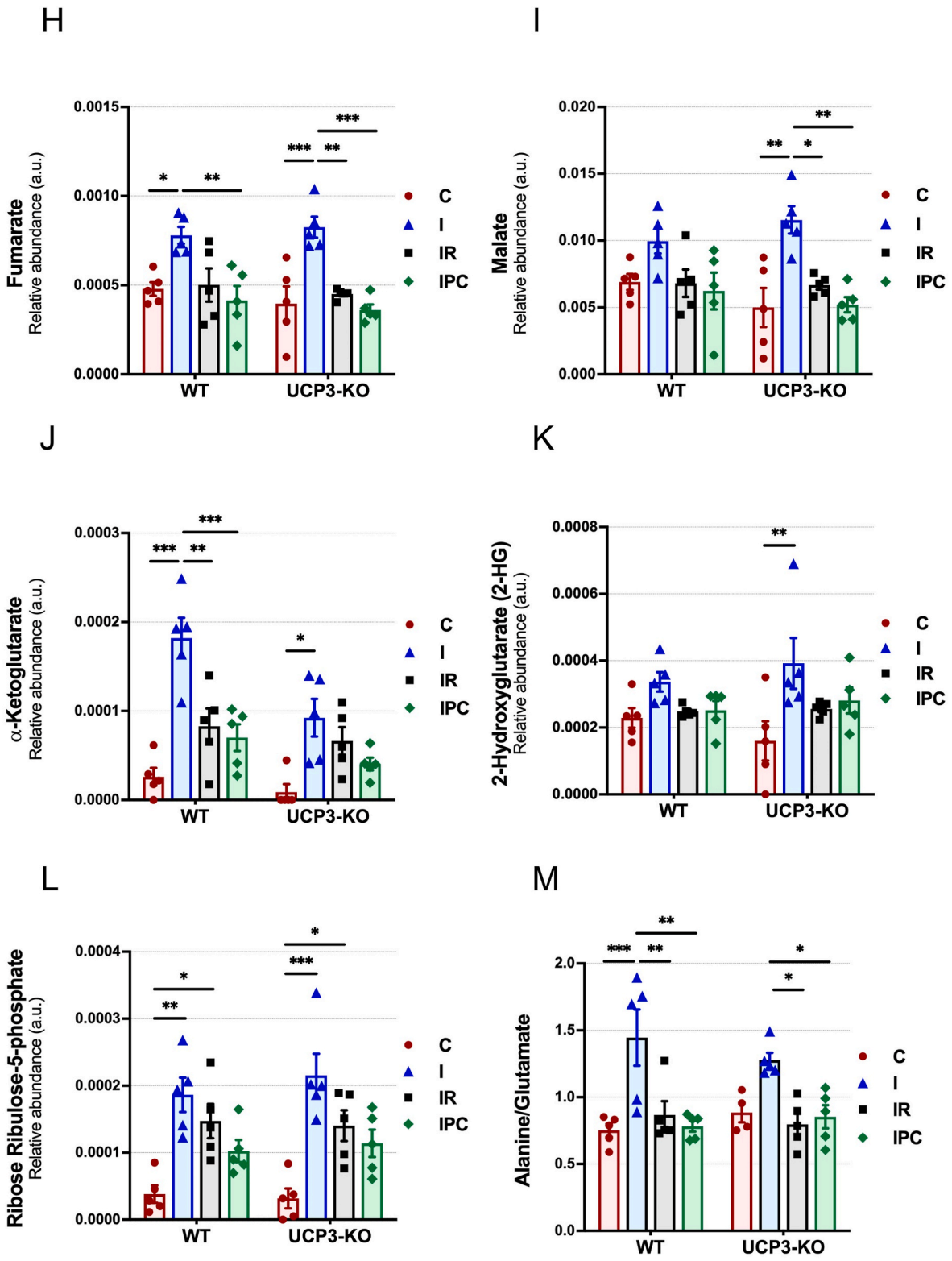

Fig. 5. (*continued*).

reflect a metabolic switch to anaerobic glucose utilization under ischemia. Anaerobic glucose utilization ceased with the reintroduction of oxygen at reperfusion, as reflected by the restoration of pre-ischemic lactate levels and an increase in glucose, which was higher than basal control levels. Reperfusion of ischemic hearts also restored succinate levels, whereas xanthine and hypoxanthine levels remained slightly higher than under the basal control condition, particularly in UCP3–KO hearts. Other intermediates of the tricarboxylic acid (TCA) cycle such as fumarate, malate, and α-ketoglutarate, also increased in abundance in ischemia and returned to basal levels upon reperfusion (Fig. 5H–J). Altogether, the data suggested that IR has an impact on the accumulation of TCA cycle intermediates in both UCP3–KO and wild-type hearts. We found an increase of 2-hydroxyglutarate in ischemia, especially in UCP3–KO hearts, and its restoration to basal levels at reperfusion

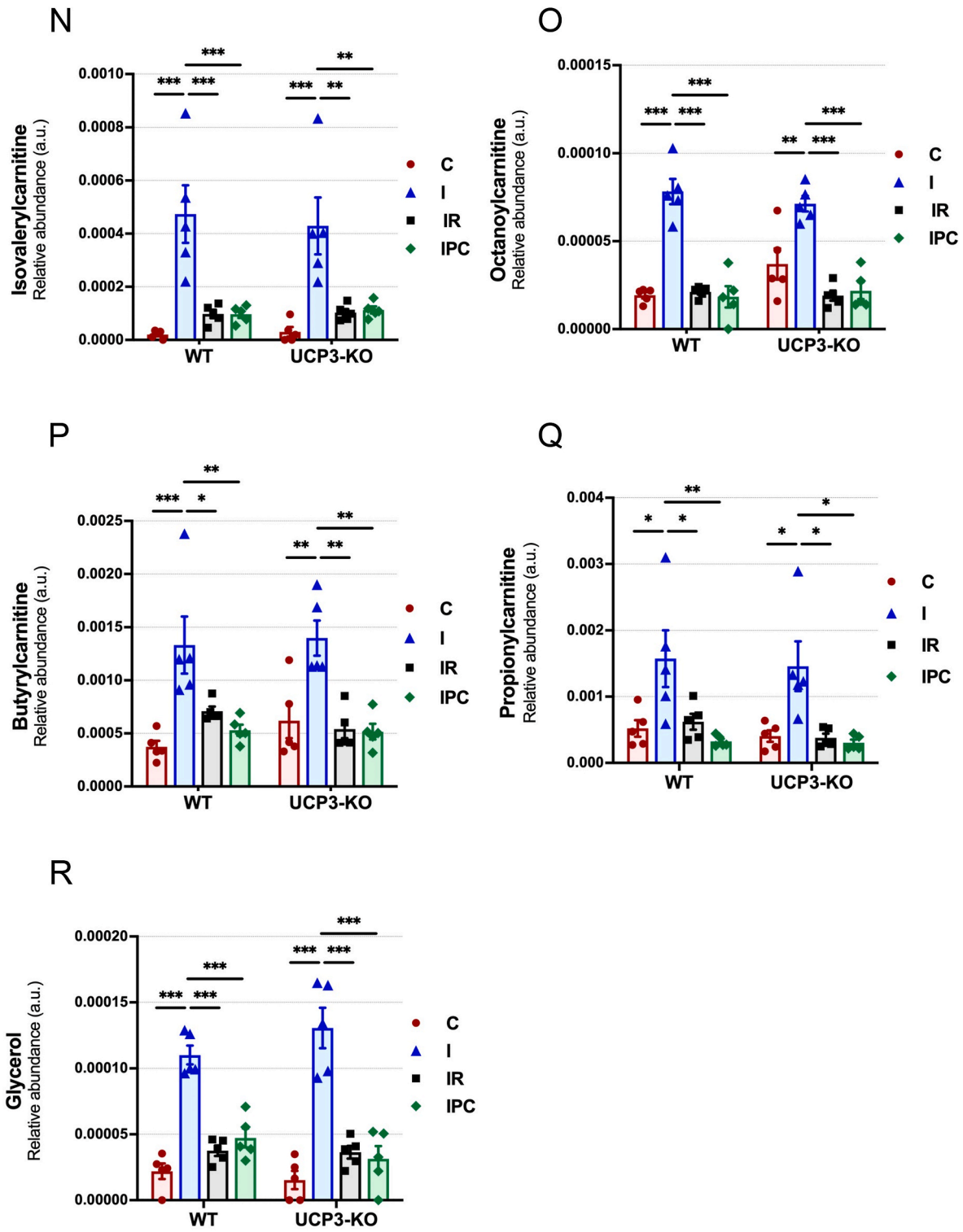

Fig. 5. (*continued*).

(Fig. 5K). Likewise, ribose-5-phosphate, an intermediate of the pentose phosphate pathway, increased in ischemia and showed a trend to decrease during reperfusion, although it remained elevated, particularly in non-preconditioned hearts (Fig. 5L). The ratio alanine/glutamate, a marker of metabolic stress, increased in ischemia and returned to basal values upon reperfusion (Fig. 5M).

The results indicated that FAO was inhibited due to the lack of oxygen during ischemia. Accordingly, several acylcarnitines, including isovalerylcarnitine, octanoylcarnitine, butyrylcarnitine and propionylcarnitine, involved in the transport of LCFAs into mitochondria for β-oxidation, accumulated in ischemia and returned to pre-ischemic levels during reperfusion (Fig. 5N–Q). A similar pattern was found for glycerol (Fig. 5R). We found a higher accumulation of the essential fatty acid linoleic acid (18:2 n-6), together with monounsaturated oleic (18:1 n-9) and palmitoleic (16:1 n-7) acids, and saturated stearic (18:0) and palmitic (16:0) acids, particularly at reperfusion, although the latter was already considerably higher during ischemia (Fig. 6S-W). Taken together, these data point to the reduced

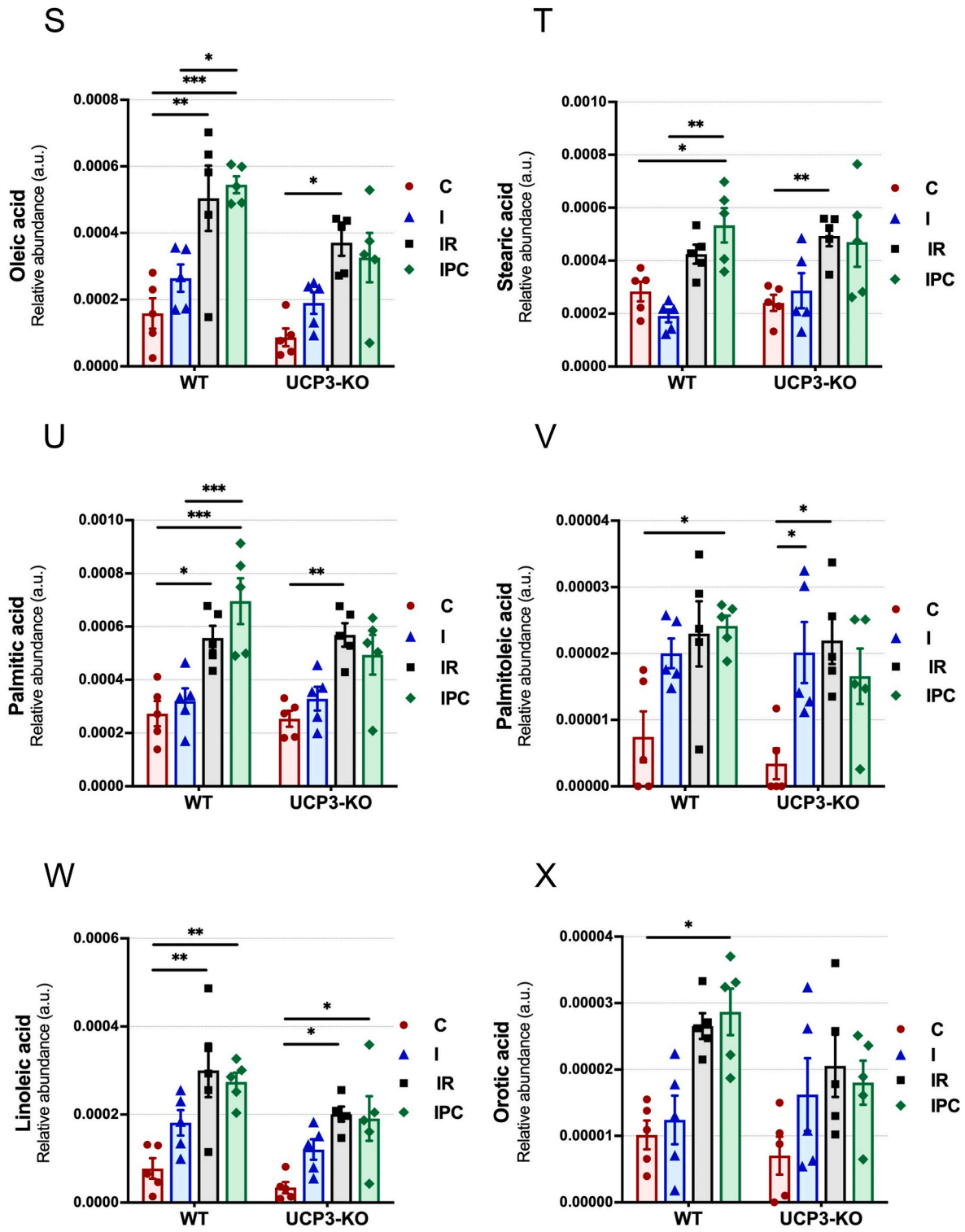

Fig. 5. (*continued*).

transport of fatty acids during ischemia and decreased β-oxidation upon reperfusion, with or without IPC. Similarly, orotic acid, an intermediate of pyrimidine biosynthesis, increased during ischemia and was even higher at reperfusion (Fig. 5X).

We found a similar pattern of elevated levels in ischemia and a return to pre-ischemic levels at reperfusion for most amino acids analyzed (Figs. S4A–E), including phenylalanine, tyrosine, leucine-isoleucine, tryptophan and histidine, reflecting a reduction in amino acid metabolism during ischemia. Creatinine, a degradation product of the amino acid derivative creatine, also increased during ischemia and decreased during reperfusion (Fig. S4F).

3.6. *IR decreases cardiac oxygen consumption similarly in UCP3–KO and wild-type hearts*

To test the hypothesis of decreased β-oxidation upon reperfusion, and to study the effects of IR on mitochondrial respiration with different substrates, we measured oxygen consumption by high-resolution

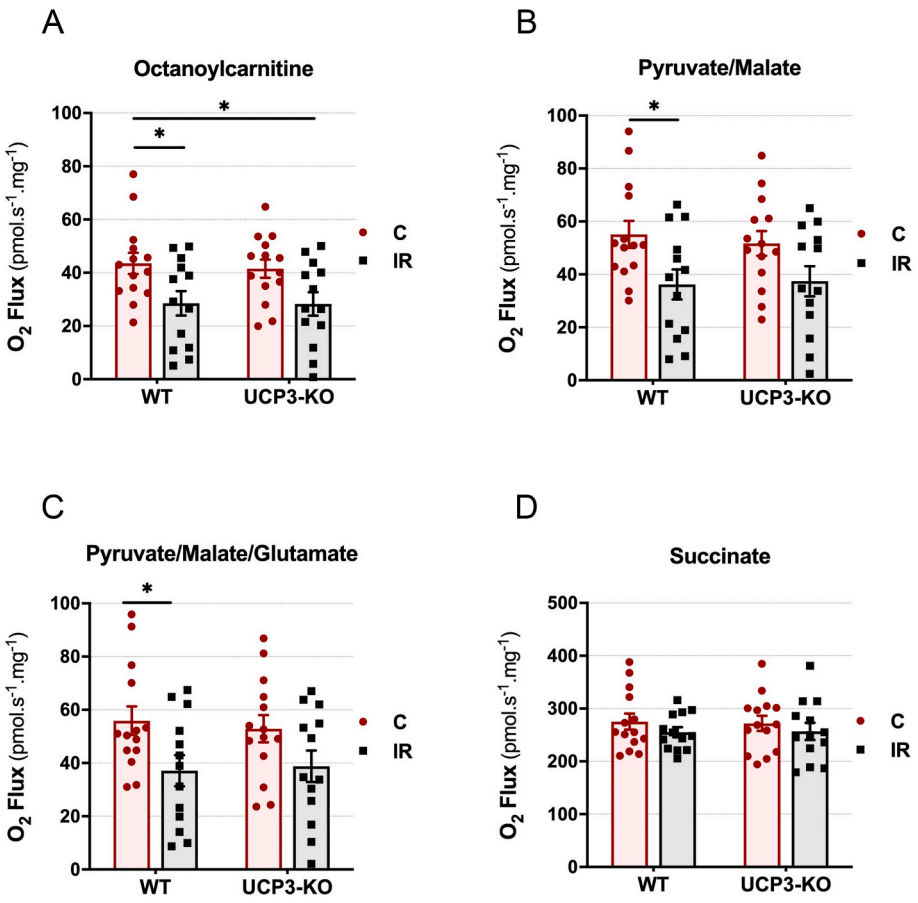

Fig. 6. Mitochondrial respiration in isolated perfused hearts from adult wild-type and UCP3–KO mice subjected to ischemia-reperfusion. Mitochondrial respiration was measured in homogenates of hearts in the presence of ADP (5 mM), $MgCl_2$ (3 mM), malate (0.5 mM) and octanoylcarnitine (750 μM) (A), pyruvate/malate (5 mM/2 mM) (B), glutamate (10 mM) (C), succinate (10 mM) (D), glycerophosphate (10 mM) (E), FCCP (1 μM) to determine maximal respiration with substrates of complex I and complex II (F), and rotenone (0.5 μM) to inhibit complex I and to determine maximal respiration with substrates of complex II (G). Calculated maximal respiration with substrates of complex I (H). Histograms show the mean ± SEM of the oxygen consumption rate (OCR; pmol.min^{-1}.mg tissue^{-1}) from 13 to 14 mice per group. Abbreviations: CI, complex I; CII, complex II; C, control; IR, ischemia-reperfusion. *$P < 0.05$.

respirometry in homogenates from wild-type and UCP3–KO hearts subjected to *ex vivo* IR. Oxygen consumption in phosphorylating conditions (in the presence of ADP) showed a trend to diminish after IR in both heart types during the oxidation of octanolylcarnitine (Fig. 6A) or with complex I substrates (pyruvate/malate; pyruvate/malate/glutamate) (Fig. 6B and C). By contrast, the addition of the complex II substrate succinate increased oxygen consumption to values similar to those of control hearts (Fig. 6D). The glycerophosphate dehydrogenase complex in the outer face of the mitochondrial inner membrane oxidizes glycerophosphate to dihydroxyacetone phosphate and feeds two electrons into the coenzyme Q. Oxygen consumption with glycerophosphate was again similar between control and IR hearts (Fig. 6E). Maximal respiration determined with FCCP was also similar between groups when mitochondria respired on complex II substrates and showed a trend to decrease after IR when respiring on complex I substrates (Fig. 6F–H). Overall, our results point to FAO and complex I-supported respiration as the most affected processes following IR in both UCP3–KO and wild-type hearts.

3.7. Viability of isolated cardiomyocytes subjected to hypoxia/reoxygenation

We studied the susceptibility of isolated cardiomyocytes to H/R by determining their viability and morphology (Fig. S5A). We found no significant differences in the number of cardiomyocytes or in the ratio of cell death (propidium iodide-positive nuclei/total nuclei) between groups (Fig. S5B-E). Eccentricity showed a trend to decrease to a similar extent in both UCP3–KO and wild-type cardiomyocytes after H/R, as reflected in a more rounded shape in damaged cells (Fig. S5F). As expected, LDH activity in the culture medium was higher in both cardiomyocyte types after H/R, although the increase was not significant (Fig. S5G).

4. Discussion

4.1. UCP3-deficient hearts are more susceptible to myocardial IR than wild-type hearts

UCP3 deficiency is known to extend myocardial injury and impair cardiac recovery after IR [40–43], and it has also been reported to increase the incidence of left ventricular diastolic dysfunction during hypertension [54]. The proposed mechanisms of UCP3-mediated cardioprotection include the regulation of myocardial energetics [41–43], ROS generation [41–43], apoptotic cell death [42], LCFA oxidation [43], and glycolytic metabolism [40]. In the present study, we found that UCP3–KO hearts develop a larger infarct area than wild-type hearts after IR, both *ex vivo* and *in vivo*. We additionally found that hearts from old UCP3–KO mice are even more vulnerable to IR injury than those from adult mice. This result could be explained by the increased susceptibility of aged hearts to IR, which is related to impaired

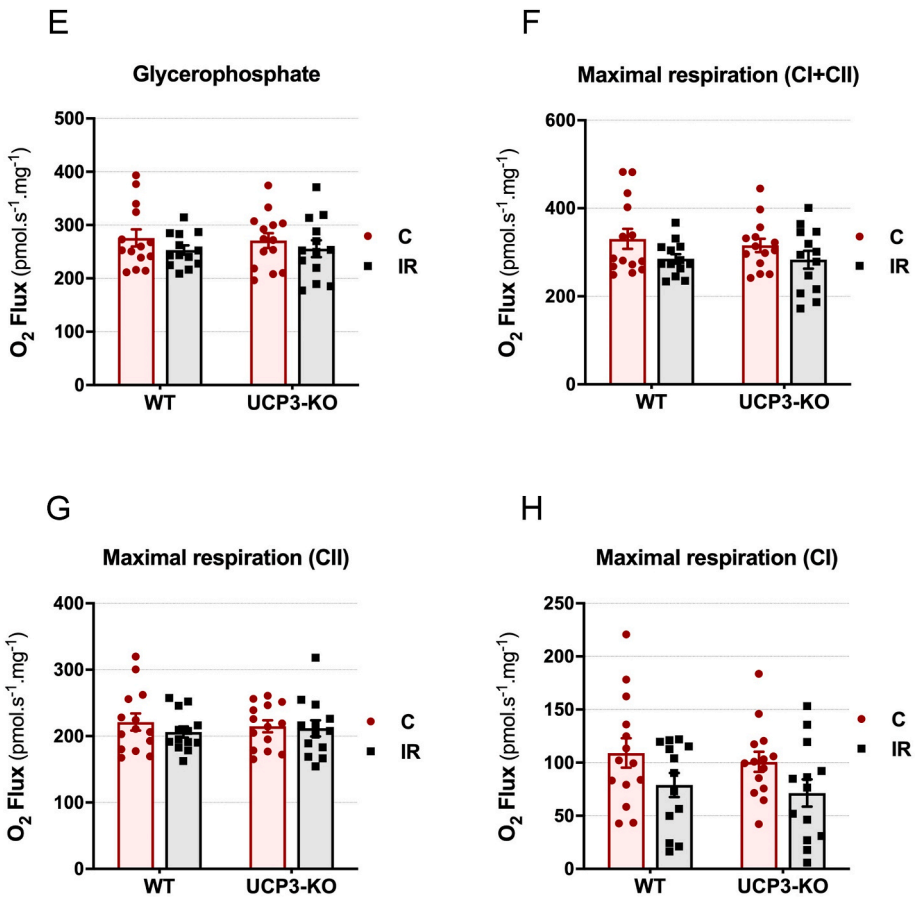

Fig. 6. (*continued*).

mitochondrial integrity in these hearts [52,53]. Moreover, histological analysis of myocardial tissue at the midventricular level revealed a larger infarct area in UCP3–KO hearts after *in vivo* IR, despite the grossly similar architecture between wild-type and UCP3–KO hearts under basal conditions [41]. Notwithstanding the clear differences in infarct size, cardiac function was not significantly different between UCP3–KO and wild-type groups, most likely due to compensatory mechanisms.

Cardiomyocytes have limited regenerative capacity in the adult heart, and many are irreversibly lost following myocardial infarction [55]. Analysis of the response of isolated cardiomyocytes to H/R revealed a similar number of cells and ratio of cell death in both groups. Also, eccentricity decreased to a similar extent in UCP3–KO and wild-type cardiomyocytes after H/R, reflected by a more rounded shape. Finally, there was a trend for an increase in the levels of LDH, a marker of cardiomyocyte damage, in both groups after H/R, but particularly in cells lacking UCP3. Overall, however, there was no clear difference in the response to H/R between wild-type cardiomyocytes and those lacking UCP3.

4.2. Increased superoxide production may account for the larger infarct size in UCP3-deficient mice

Reperfusion injury has long been associated with a burst of mitochondrial ROS [56,57], particularly from respiratory complex I [7,8,58]. During reperfusion, a highly reduced coenzyme Q pool and a high protonmotive force to drive RET support the generation of superoxide/hydrogen peroxide from the I_Q site of complex I [59,60]. Succinate accumulates during ischemia, and can act as an electron donor for RET during reperfusion [7,8]. Mild uncoupling of oxidative phosphorylation mediated by UCP2 and UCP3 has been proposed as a mechanism to limit excessive superoxide production from the electron transport chain [25,26]. Our analysis of mitochondrial matrix with MitoB revealed similar levels of H_2O_2 in both heart types 15 min after reperfusion. We can speculate that an enhanced production of superoxide/H_2O_2 occurs earlier during reperfusion in hearts lacking UCP3. A second approach to determine whether an augmented superoxide production could account for the greater damage in UCP3–KO hearts was to test the effect of a superoxide suppressor on infarct size and CK activity after IR. S1QEL suppresses superoxide production during RET through the I_Q site without affecting oxidative phosphorylation [61]. Previous reports have shown that the inclusion of S1QEL at the time of reperfusion improves post-ischemic recovery of cardiac function, and significantly reduces infarct size [62]. Our results revealed a trend for a decrease in infarct size and CK activity with S1QEL, but only in UCP3–KO heart, suggesting that the greater damage in these hearts could be due, at least in part, to increased mitochondrial superoxide production from site I_Q, and supporting the prevailing notion that UCP3 modulates mitochondrial superoxide production.

4.3. Lipid and energy metabolism are the most affected pathways after myocardial ex vivo IR

A recent comparative metabolomics analysis in different tissues subjected to IR revealed a substantial accumulation of three metabolites: hypoxathine, xanthine and succinate [8]. Both xanthine and hypoxanthine accumulate during ischemia due to the breakdown of purine nucleotides by the purine nucleotide cycle in response to ischemic AMP accumulation [8,63]. Xanthine oxidoreductase is an important source of ROS and related post-ischemic injury [64,65]. Oxygen availability during reperfusion promotes the oxidation of hypoxanthine to uric acid, while molecular oxygen is concomitantly reduced to superoxide (Fig. 6B). Our results in *ex vivo* perfused hearts show that these

metabolites accumulate in ischemia to a similar extent in wild-type and UCP3–KO mice, and return to near pre-ischemic values at reperfusion. We also found a similar elevation of the ratio alanine/glutamate, a marker of metabolic stress, which has been reported to increase during cardiac ischemia [66,67].

The lack of oxygen during ischemia shifts cardiac metabolism from the mitochondrial oxidation of fatty acids and carbohydrates to anaerobic glycolysis, which disrupts mitochondrial ATP generation and reduces overall ATP availability [4]. During ischemia, the myocardium becomes a net lactate producer due to accelerated glycolysis in the presence of impaired pyruvate oxidation [68]. Our results show that cardiac metabolism shifts to glycolysis in response to IR, as reflected by a decrease in glucose and an increased in lactate. Notably, glucose levels have been reported to remain high during reperfusion [69], which indicates the delayed recovery of glycolysis. As mentioned earlier, succinate is a universal metabolic marker of ischemia [8]. We found that succinate accumulated in ischemia particularly in UCP3–KO mice, and returned to basal levels upon reperfusion, which could be explained by either its efflux [70] or its catabolism [8]. The origin of succinate accumulation in ischemia remains contentious. Chouchani et al. proposed that succinate accumulation occurs from reversal of succinate dehydrogenase (complex II) under ischemia, which in turn is driven by fumarate overflow from purine nucleotide breakdown and partial reversal of the malate/aspartate shuttle [8]. Following reperfusion, the accumulated succinate is rapidly re-oxidized by succinate dehydrogenase, which acutely drives extensive superoxide generation by RET at mitochondrial complex I. Other authors, however, propose that succinate accumulates from canonical TCA cycle activity (i.e., from the conversion of α-ketoglutarate to succinate *via* succinyl-CoA) [71,72]. Our results do not allow us to discriminate between these models, but they confirm the accumulation of succinate in ischemia and the lack of an effect of IPC on succinate accumulation or its oxidation at reperfusion [73]. Other intermediates of the TCA cycle such as fumarate, malate, and α-ketoglutarate also accumulated in ischemia. We also found increased levels of 2-hydroxyglutarate. This metabolite, generated by the promiscuous action of malate dehydrogenase and lactate dehydrogenase (LDH) on α-ketoglutarate, accumulates in ischemia and has been recently shown to protect against cardiac IR injury through a metabolic shift of glucose flux from glycolysis to the pentose phosphate pathway [74]. Ribose-5-phosphate, an intermediate of the pentose phosphate pathway, also accumulated in ischemia. This metabolite can be used for nucleotide synthesis and can participate in the repletion of the ATP pool during recovery from ischemia [75].

Our results point to fatty acid metabolism as one of the pathways most affected by IR in both UCP3–KO and wild-type hearts, as shown by the accumulation of several carnitine species, such as isovalerylcarnitine, octanoylcarnitine, butyrylcarnitine, and propionylcarnitine, in ischemia. Likewise, the levels of several fatty acids were elevated in ischemia to different degrees and increased further during reperfusion. In some cases, the accumulation was greater in wild-type hearts than in UCP3–KO hearts, especially after IPC. It is well established that, during global ischemia, the inhibition of FAO owing to the lack of oxygen and the accumulation of reducing equivalents (NADH and $FADH_2$) can result in the accumulation of fatty acid intermediates in different cellular compartments [76]. Fatty acylcarnitine species can accumulate in both the mitochondrial matrix and the cytosol, whereas fatty acyl CoA species accumulate mainly in the mitochondrial matrix [77,78]. The accumulation of these acylcarnitine and acyl-CoA esters is associated with increased ROS production and oxidative stress, and promotes disruption of mitochondria cristae and the formation of amorphous intramitochondrial densities, which may ultimately disturb mitochondrial function [79–81]. We detected these types of alterations by microscopy (see below). Of note, breakdown of triacylglycerols and disruption of membrane lipids during reperfusion could be responsible for the elevation of fatty acids, as the perfusion buffer did not contain fatty acids. This may be a possible limitation of this study, since it might lead to underestimation of fatty acid metabolism-derived substrate concentrations. Glycerol also accumulated in ischemic hearts, likely originating from lipolysis of intracellular triacylglycerols, hydrolysis of glycerol-3-phosphate produced by glycolysis, and degradation of membrane phospholipids. Indeed, glycerol release is considered as a marker of ischemic metabolism and as an indicator of reperfusion injury [82]. Our results indicate that fatty acid metabolism is equally affected in wild-type and UCP3–KO mice after *ex vivo* IR, which supports the view that UCP3 is not required for FAO or fatty acid transport, although it might be involved in mitochondrial adaptation to fasting, possibly by reducing oxidative stress [36].

Orotic acid is an intermediate of pyrimidine biosynthesis and, therefore, may affect several biochemical processes that involve pyrimidine nucleotides, such as the biosynthesis of RNA, glycogen, and phospholipids. Orotic acid followed the same pattern as fatty acids: elevated levels in ischemia and higher levels at reperfusion, particularly in wild-type hearts. Orotic acid has been shown to improve cardiac performance after IR, likely by increasing the myocardial glycogen content [83]. We found increased levels of the essential amino acids leucine, histidine and the aromatic amino acids phenylalanine, tyrosine and tryptophan in ischemic hearts from both wild-type and UCP3–KO mice, which was more evident in UCP3–KO mice. Interestingly, UCP3 overexpression in muscle regulates biochemical pathways associated with amino acid metabolism and redox status, which impacts other organ systems [84]. Finally, creatinine, a by-product of muscle metabolism, was elevated in ischemia, particularly in UCP3–KO hearts, and decreased again during reperfusion, reflecting ischemic cardiac dysfunction.

4.4. Myocardial ex vivo IR impairs respiration with the medium-chain fatty acid octanoate and with complex I substrates in both UCP3-deficient and wild-type hearts

Bioenergetics analysis of heart homogenates revealed that ADP-stimulated respiration is impaired in hearts subjected to *ex vivo* IR respiring on octanoylcarnitine (the carnitine-bound form of the medium-chain fatty acid octanoate) and on substrates of complex I (pyruvate/malate/glutamate), but not on substrates of complex II (succinate) or glycerophosphate. Likewise, maximal respiration with complex I substrates showed a trend for a decrease in both heart types after IR. These results agree with those reported by Edwards et al., who showed that mitochondria isolated from rats with partial loss of UCP3 ($ucp3^{+/-}$) have lower ADP-stimulated respiration with oleate and complex I (but not complex II) substrates after IR [43]. However, they reported that respiration was lower (16% decrease) with oleate or complex I substrates in $ucp3^{+/-}$ mitochondria than in wild-type mitochondria, which we did not detect. Differences in the model used (mouse *vs* rat), sex (male *vs* both male and female), IR protocol (*ex vivo* 40 min ischemia/60 min reperfusion *vs in vivo* 15 min ischemia/45 min reperfusion), experimental design (heart homogenates *vs* isolated mitochondria), or the fatty acid used as substrate (medium-chain octanoic acid *vs* long-chain oleate) likely account for the discrepancies. Nevertheless, our results agree with the idea that complex I is severely affected by IR [85–87]. This dysfunction has been attributed to mitochondrial calcium uptake [85], ROS-induced cardiolipin damage [87], and/or cysteine sulfonation [86]. In addition, the impairment in FAO that we observed in homogenates of hearts subjected to IR is in accord with the accumulation of fatty acids detected in our metabolic analysis.

4.5. Mitochondrial structure is severely affected by ex vivo IR in UCP3-deficient mice

The heart adapts to stress through metabolic and structural remodeling. We have found that *ex vivo* IR alters mitochondrial structure, especially in UCP3–KO hearts. After IR, a considerable fraction of mitochondria appeared more fragmented, with a decrease in the number

of mitochondrial junctions and an accumulation of lipid droplets. These morphological changes have been previously observed in UCP3–KO mice following permanent coronary artery ligation [42], and might contribute to myocardial IR injury. Indeed, inhibiting mitochondrial fission protects the rodent heart against IR injury [88]. Myocardial IR can lead to the increased accumulation of lipids and lipid metabolites that have toxic effects on cardiomyocytes, ultimately impairing myocardial function [89]. Interestingly, we found that the mitochondrial ultrastructure of UCP3–KO perfused hearts was impaired under basal conditions. Similar morphological changes have been recently reported in brown adipose tissue lacking UCP3 [90]. Overall, our electron microscopy analysis points to a role of UCP3 as a guardian of mitochondrial structure.

In summary, we confirm that hearts from mice lacking UCP3 are more susceptible to *ex vivo* and *in vivo* IR injury than those from wild-type mice, and we show that this is more significant in older mice. Our data using S1QEL indicate that superoxide generated from site I_Q in complex I might be relevant for the greater cardiomyocyte damage in hearts lacking UCP3. The metabolic response to ischemia and IR is, however, quite similar in both types of hearts, with lipid and energy metabolism emerging as the most affected pathways. FAO and complex I (but not complex II) function are impaired after IR. The lack of UCP3 promotes important mitochondrial ultrastructural changes after IR, likely due to increased ROS or lipotoxicity, and affects the number of inter-mitochondrial junctions and the accumulation of lipid droplets. Further research is needed to clarify the origin of these structural alterations and to guide UCP3-related strategies that could help reduce cardiac damage after IR.

Declaration of competing interest

The authors declare that no competing financial interests exist in relation to this manuscript.

Acknowledgements

We are grateful to F. Sánchez-Madrid, B. Ibáñez and E. Lara for facilitating experiments at CNIC (Madrid, Spain) and to W.E. Louch for facilitating experiments at the University of Oslo (Oslo, Norway). We thank B. Littlejohns, I. Khaliulin and H. Lin from M.S. Suleiman's group (University of Bristol, Bristol, UK) for their valuable help with Langendorff perfusion experiments. We also thank E.T. Chouchani from M.P. Murphy's group (Cambridge, UK) for help with metabolomics analysis, M. Guerra of the Electron Microscopy Unit at CBMSO (Madrid, Spain) for processing the samples for electron microscopy analysis, and A.V. Alonso (CNIC) for echocardiography analyses. The work in our laboratory is funded the Instituto de Salud Carlos III (FIS PI19/01030) to SC. Institutional grants from the Fundación Ramón Areces and Banco de Santander to the CBMSO are also acknowledged.

Appendix A. Supplementary data

Supplementary data to this article can be found online at https://doi.org/10.1016/j.freeradbiomed.2023.05.014.

References

[1] L. Schirone, M. Forte, L. D'Ambrosio, V. Valenti, D. Vecchio, S. Schiavon, G. Spinosa, G. Sarto, V. Petrozza, G. Frati, S. Sciarretta, An overview of the molecular mechanisms associated with myocardial ischemic injury: state of the art and translational perspectives, Cells 11 (2022) 1165, https://doi.org/10.3390/cells11071165.

[2] G. Pedriali, D. Ramaccini, E. Bouhamida, M.R. Wieckowski, C. Giorgi, E. Tremoli, P. Pinton, Perspectives on mitochondrial relevance in cardiac ischemia/reperfusion injury, Front. Cell Dev. Biol. 10 (2022), 1082095, https://doi.org/10.3389/fcell.2022.1082095.

[3] S. Cadenas, ROS and redox signaling in myocardial ischemia-reperfusion injury and cardioprotection, Free Radic. Biol. Med. 117 (2018) 76–89, https://doi.org/10.1016/j.freeradbiomed.2018.01.024.

[4] D.J. Hausenloy, D.M. Yellon, Myocardial ischemia-reperfusion injury: a neglected therapeutic target, J. Clin. Invest. 123 (2013) 92–100, https://doi.org/10.1172/JCI62874.

[5] E.J. Lesnefsky, S. Moghaddas, B. Tandler, J. Kerner, C.L. Hoppel, Mitochondrial dysfunction in cardiac disease: ischemia–reperfusion, aging, and heart failure, J. Mol. Cell. Cardiol. 33 (2001) 1065–1089, https://doi.org/10.1006/jmcc.2001.1378.

[6] D.N. Granger, P.R. Kvietys, Reperfusion injury and reactive oxygen species: the evolution of a concept, Redox Biol. 6 (2015) 524–551, https://doi.org/10.1016/j.redox.2015.08.020.

[7] E.T. Chouchani, V.R. Pell, A.M. James, L.M. Work, K. Saeb-Parsy, C. Frezza, T. Krieg, M.P. Murphy, A unifying mechanism for mitochondrial superoxide production during ischemia-reperfusion injury, Cell Metabol. 23 (2016) 254–263, https://doi.org/10.1016/j.cmet.2015.12.009.

[8] E.T. Chouchani, V.R. Pell, E. Gaude, D. Aksentijević, S.Y. Sundier, E.L. Robb, A. Logan, S.M. Nadtochiy, E.N.J. Ord, A.C. Smith, F. Eyassu, R. Shirley, C.-H. Hu, A. J. Dare, A.M. James, S. Rogatti, R.C. Hartley, S. Eaton, A.S.H. Costa, P.S. Brookes, S.M. Davidson, M.R. Duchen, K. Saeb-Parsy, M.J. Shattock, A.J. Robinson, L. M. Work, C. Frezza, T. Krieg, M.P. Murphy, Ischaemic accumulation of succinate controls reperfusion injury through mitochondrial ROS, Nature 515 (2014) 431–435, https://doi.org/10.1038/nature13909.

[9] Q. Chen, S. Moghaddas, C.L. Hoppel, E.J. Lesnefsky, Reversible blockade of electron transport during ischemia protects mitochondria and decreases myocardial injury following reperfusion, J. Pharmacol. Exp. Therapeut. 319 (2006) 1405–1412, https://doi.org/10.1124/jpet.106.110262.

[10] S. Cadenas, Mitochondrial uncoupling, ROS generation and cardioprotection, Biochim. Biophys. Acta Bioenerg. 1859 (2018) 940–950, https://doi.org/10.1016/j.bbabio.2018.05.019.

[11] J. Minners, E.J. van den Bos, D.M. Yellon, H. Schwalb, L.H. Opie, M.N. Sack, Dinitrophenol, cyclosporin A, and trimetazidine modulate preconditioning in the isolated rat heart: support for a mitochondrial role in cardioprotection, Cardiovasc. Res. 47 (2000) 68–73, https://doi.org/10.1016/s0008-6363(00)00069-9.

[12] J.P. Brennan, R. Southworth, R.A. Medina, S.M. Davidson, M.R. Duchen, M. J. Shattock, Mitochondrial uncoupling, with low concentration FCCP, induces ROS-dependent cardioprotection independent of KATP channel activation, Cardiovasc. Res. 72 (2006) 313–321, https://doi.org/10.1016/j.cardiores.2006.07.019.

[13] J.P. Brennan, R.G. Berry, M. Baghai, M.R. Duchen, M.J. Shattock, FCCP is cardioprotective at concentrations that cause mitochondrial oxidation without detectable depolarisation, Cardiovasc. Res. 72 (2006) 322–330, https://doi.org/10.1016/j.cardiores.2006.08.006.

[14] D.W. Gong, S. Monemdjou, O. Gavrilova, L.R. Leon, B. Marcus-Samuels, C.J. Chou, C. Everett, L.P. Kozak, C. Li, C. Deng, M.E. Harper, M.L. Reitman, Lack of obesity and normal response to fasting and thyroid hormone in mice lacking uncoupling protein-3, J. Biol. Chem. 275 (2000) 16251–16257, https://doi.org/10.1074/jbc.M910177199.

[15] A.J. Vidal-Puig, D. Grujic, C.Y. Zhang, T. Hagen, O. Boss, Y. Ido, A. Szczepanik, J. Wade, V. Mootha, R. Cortright, D.M. Muoio, B.B. Lowell, Energy metabolism in uncoupling protein 3 gene knockout mice, J. Biol. Chem. 275 (2000) 16258–16266, https://doi.org/10.1074/jbc.M910179199.

[16] A. Lombardi, R.A. Busiello, L. Napolitano, F. Cioffi, M. Moreno, P. de Lange, E. Silvestri, A. Lanni, F. Goglia, UCP3 translocates lipid hydroperoxide and mediates lipid hydroperoxide-dependent mitochondrial uncoupling, J. Biol. Chem. 285 (2010) 16599–16605, https://doi.org/10.1074/jbc.M110.102699.

[17] S. Cadenas, J.A. Buckingham, S. Samec, J. Seydoux, N. Din, A.G. Dulloo, M. D. Brand, UCP2 and UCP3 rise in starved rat skeletal muscle but mitochondrial proton conductance is unchanged, FEBS Lett. 462 (1999) 257–260, https://doi.org/10.1016/s0014-5793(99)01540-9.

[18] V. Bézaire, W. Hofmann, J.K. Kramer, L.P. Kozak, M.E. Harper, Effects of fasting on muscle mitochondrial energetics and fatty acid metabolism in Ucp3(-/-) and wild-type mice, Am. J. Physiol. Endocrinol. Metab. 281 (2001) E975–E982, https://doi.org/10.1152/ajpendo.2001.281.5.E975.

[19] S. Cadenas, K.S. Echtay, J.A. Harper, M.B. Jekabsons, J.A. Buckingham, E. Grau, A. Abuin, H. Chapman, J.C. Clapham, M.D. Brand, The basal proton conductance of skeletal muscle mitochondria from transgenic mice overexpressing or lacking uncoupling protein-3, J. Biol. Chem. 277 (2002) 2773–2778, https://doi.org/10.1074/jbc.M109736200.

[20] E. Aguirre, S. Cadenas, GDP and carboxyatractylate inhibit 4-hydroxynonenal-activated proton conductance to differing degrees in mitochondria from skeletal muscle and heart, Biochim. Biophys. Acta 1797 (2010) 1716–1726, https://doi.org/10.1016/j.bbabio.2010.06.009.

[21] M.D. Brand, R. Pamplona, M. Portero-Otín, J.R. Requena, S.J. Roebuck, J. A. Buckingham, J.C. Clapham, S. Cadenas, Oxidative damage and phospholipid fatty acyl composition in skeletal muscle mitochondria from mice underexpressing or overexpressing uncoupling protein 3, Biochem. J. 368 (2002) 597–603, https://doi.org/10.1042/BJ20021077.

[22] L.J. Toime, M.D. Brand, Uncoupling protein-3 lowers reactive oxygen species production in isolated mitochondria, Free Radic. Biol. Med. 49 (2010) 606–611, https://doi.org/10.1016/j.freeradbiomed.2010.05.010.

[23] M.D. Brand, T.C. Esteves, Physiological functions of the mitochondrial uncoupling proteins UCP2 and UCP3, Cell Metabol. 2 (2005) 85–93, https://doi.org/10.1016/j.cmet.2005.06.002.

[24] R.J. Mailloux, M.-E. Harper, Uncoupling proteins and the control of mitochondrial reactive oxygen species production, Free Radic. Biol. Med. 51 (2011) 1106–1115, https://doi.org/10.1016/j.freeradbiomed.2011.06.022.
[25] M.P. Murphy, K.S. Echtay, F.H. Blaikie, J. Asin-Cayuela, H.M. Cocheme, K. Green, J.A. Buckingham, E.R. Taylor, F. Hurrell, G. Hughes, S. Miwa, C.E. Cooper, D. A. Svistunenko, R.A.J. Smith, M.D. Brand, Superoxide activates uncoupling proteins by generating carbon-centered radicals and initiating lipid peroxidation: studies using a mitochondria-targeted spin trap derived from alpha-phenyl-N-tert-butylnitrone, J. Biol. Chem. 278 (2003) 48534–48545, https://doi.org/10.1074/jbc.M308529200.
[26] K.S. Echtay, D. Roussel, J. St-Pierre, M.B. Jekabsons, S. Cadenas, J.A. Stuart, J. A. Harper, S.J. Roebuck, A. Morrison, S. Pickering, J.C. Clapham, M.D. Brand, Superoxide activates mitochondrial uncoupling proteins, Nature 415 (2002) 96–99, https://doi.org/10.1038/415096a.
[27] D.G. Nicholls, The physiological regulation of uncoupling proteins, Biochim. Biophys. Acta 1757 (2006) 459–466, https://doi.org/10.1016/j.bbabio.2006.02.005.
[28] B. Cannon, I.G. Shabalina, T.V. Kramarova, N. Petrovic, J. Nedergaard, Uncoupling proteins: a role in protection against reactive oxygen species–or not? Biochim. Biophys. Acta 1757 (2006) 449–458, https://doi.org/10.1016/j.bbabio.2006.05.016.
[29] E. López-Bernardo, A. Anedda, P. Sánchez-Pérez, B. Acosta-Iborra, S. Cadenas, 4-Hydroxynonenal induces Nrf2-mediated UCP3 upregulation in mouse cardiomyocytes, Free Radic. Biol. Med. 88 (2015) 427–438, https://doi.org/10.1016/j.freeradbiomed.2015.03.032.
[30] A. Anedda, E. López-Bernardo, B. Acosta-Iborra, M. Saadeh Suleiman, M. O. Landázuri, S. Cadenas, The transcription factor Nrf2 promotes survival by enhancing the expression of uncoupling protein 3 under conditions of oxidative stress, Free Radic. Biol. Med. 61 (2013) 395–407, https://doi.org/10.1016/j.freeradbiomed.2013.04.007.
[31] R.J. Mailloux, E.L. Seifert, F. Bouillaud, C. Aguer, S. Collins, M.-E. Harper, Glutathionylation acts as a control switch for uncoupling proteins UCP2 and UCP3, J. Biol. Chem. 286 (2011) 21865–21875, https://doi.org/10.1074/jbc.M111.240242.
[32] S. Brun, M.C. Carmona, T. Mampel, O. Viñas, M. Giralt, R. Iglesias, F. Villarroya, Activators of peroxisome proliferator-activated receptor-alpha induce the expression of the uncoupling protein-3 gene in skeletal muscle: a potential mechanism for the lipid intake-dependent activation of uncoupling protein-3 gene expression at birth, Diabetes 48 (1999) 1217–1222, https://doi.org/10.2337/diabetes.48.6.1217.
[33] P. Schrauwen, J. Hoeks, G. Schaart, E. Kornips, B. Binas, G.J. Van De Vusse, M. Van Bilsen, J.J.F.P. Luiken, S.L.M. Coort, J.F.C. Glatz, W.H.M. Saris, M.K.C. Hesselink, Uncoupling protein 3 as a mitochondrial fatty acid anion exporter, Faseb. J. 17 (2003) 2272–2274, https://doi.org/10.1096/fj.03-0515fje.
[34] E.J. Anderson, H. Yamazaki, P.D. Neufer, Induction of endogenous uncoupling protein 3 suppresses mitochondrial oxidant emission during fatty acid-supported respiration, J. Biol. Chem. 282 (2007) 31257–31266, https://doi.org/10.1074/jbc.M706129200.
[35] J.D. MacLellan, M.F. Gerrits, A. Gowing, P.J.S. Smith, M.B. Wheeler, M.-E. Harper, Physiological increases in uncoupling protein 3 augment fatty acid oxidation and decrease reactive oxygen species production without uncoupling respiration in muscle cells, Diabetes 54 (2005) 2343–2350, https://doi.org/10.2337/diabetes.54.8.2343.
[36] E.L. Seifert, V. Bézaire, C. Estey, M.-E. Harper, Essential role for uncoupling protein-3 in mitochondrial adaptation to fasting but not in fatty acid oxidation or fatty acid anion export, J. Biol. Chem. 283 (2008) 25124–25131, https://doi.org/10.1074/jbc.M803871200.
[37] R.J. Mailloux, T. Dumouchel, C. Aguer, R. deKemp, R. Beanlands, M.-E. Harper, Hexokinase II acts through UCP3 to suppress mitochondrial reactive oxygen species production and maintain aerobic respiration, Biochem. J. 437 (2011) 301–311, https://doi.org/10.1042/BJ20110571.
[38] T. Hamada, K. Kotani, S. Fujiwara, Y. Sano, M. Domichi, K. Tsuzaki, N. Sakane, The common -55 C/T polymorphism in the promoter region of the uncoupling protein 3 gene reduces prevalence of obesity and elevates serum high-density lipoprotein cholesterol levels in the general Japanese population, Metabolism 57 (2008) 410–415, https://doi.org/10.1016/j.metabol.2007.10.019.
[39] C.B. Chan, M.-E. Harper, Uncoupling proteins: role in insulin resistance and insulin insufficiency, Curr. Diabetes Rev. 2 (2006) 271–283, https://doi.org/10.2174/157339906777950660.
[40] S. Gargiulo, M.P. Petretta, A. Greco, M. Panico, M. Larobina, M. Gramanzini, G. G. Schiattarella, G. Esposito, M. Petretta, A. Brunetti, A. Cuocolo, Genetic deletion in uncoupling protein 3 augments 18F-fluorodeoxyglucose cardiac uptake in the ischemic heart, BMC Cardiovasc. Disord. 14 (2014) 98, https://doi.org/10.1186/1471-2261-14-98.
[41] C. Ozcan, M. Palmeri, T.L. Horvath, K.S. Russell, R.R. Russell, Role of uncoupling protein 3 in ischemia-reperfusion injury, arrhythmias, and preconditioning, Am. J. Physiol. Heart Circ. Physiol. 304 (2013) H1192–H1200, https://doi.org/10.1152/ajpheart.00592.2012.
[42] C. Perrino, G.G. Schiattarella, A. Sannino, G. Pironti, M.P. Petretta, A. Cannavo, G. Gargiulo, F. Ilardi, F. Magliulo, A. Franzone, G. Carotenuto, F. Serino, G. G. Altobelli, V. Cimini, A. Cuocolo, A. Lombardi, F. Goglia, C. Indolfi, B. Trimarco, G. Esposito, Genetic deletion of uncoupling protein 3 exaggerates apoptotic cell death in the ischemic heart leading to heart failure, J. Am. Heart Assoc. 2 (2013), e000086, https://doi.org/10.1161/JAHA.113.000086.
[43] K.S. Edwards, S. Ashraf, T.M. Lomax, J.M. Wiseman, M.E. Hall, F.N. Gava, J. E. Hall, J.P. Hosler, R. Harmancey, Uncoupling protein 3 deficiency impairs myocardial fatty acid oxidation and contractile recovery following ischemia/reperfusion, Basic Res. Cardiol. 113 (2018) 47, https://doi.org/10.1007/s00395-018-0707-9.
[44] J.W. Song, H.J. Kim, H. Lee, J. Kim, Y.-L. Kwak, Protective effect of peroxisome proliferator-activated receptor α activation against cardiac ischemia-reperfusion injury is related to upregulation of uncoupling protein-3, Oxid. Med. Cell. Longev. (2016), 3539649, https://doi.org/10.1155/2016/3539649, 2016.
[45] A. Gentile, N. Magnacca, R. de Matteis, M. Moreno, F. Cioffi, A. Giacco, A. Lanni, P. de Lange, R. Senese, F. Goglia, E. Silvestri, A. Lombardi, Ablation of uncoupling protein 3 affects interrelated factors leading to lipolysis and insulin resistance in visceral white adipose tissue, Faseb. J. 36 (2022), e22325, https://doi.org/10.1096/fj.202101816RR.
[46] M.M. López-Olañeta, M. Villalba, J.M. Gómez-Salinero, L.J. Jiménez-Borreguero, R. Breckenridge, P. Ortiz-Sánchez, P. García-Pavía, B. Ibáñez, E. Lara-Pezzi, Induction of the calcineurin variant CnAβ1 after myocardial infarction reduces post-infarction ventricular remodelling by promoting infarct vascularization, Cardiovasc. Res. 102 (2014) 396–406, https://doi.org/10.1093/cvr/cvu068.
[47] R.M. Lang, M. Bierig, R.B. Devereux, F.A. Flachskampf, E. Foster, P.A. Pellikka, M. H. Picard, M.J. Roman, J. Seward, J.S. Shanewise, S.D. Solomon, K.T. Spencer, M.S. J. Sutton, W.J. Stewart, Chamber Quantification Writing Group, American society of echocardiography's guidelines and standards committee, European association of echocardiography, recommendations for chamber quantification: a report from the American society of echocardiography's guidelines and standards committee and the chamber quantification writing group, developed in conjunction with the European association of echocardiography, a branch of the European society of cardiology, J. Am. Soc. Echocardiogr. 18 (2005) 1440–1463, https://doi.org/10.1016/j.echo.2005.10.005.
[48] L. Scorrano, M. Ashiya, K. Buttle, S. Weiler, S.A. Oakes, C.A. Mannella, S. J. Korsmeyer, A distinct pathway remodels mitochondrial cristae and mobilizes cytochrome c during apoptosis, Dev. Cell 2 (2002) 55–67, https://doi.org/10.1016/s1534-5807(01)00116-2.
[49] M. Picard, M.J. McManus, G. Csordás, P. Várnai, G.W. Dorn, D. Williams, G. Hajnóczky, D.C. Wallace, Trans-mitochondrial coordination of cristae at regulated membrane junctions, Nat. Commun. 6 (2015) 6259, https://doi.org/10.1038/ncomms7259.
[50] T.D. O'Connell, M.C. Rodrigo, P.C. Simpson, Isolation and culture of adult mouse cardiac myocytes, Methods Mol. Biol. 357 (2007) 271–296, https://doi.org/10.1385/1-59745-214-9:271.
[51] L. Kamentsky, T.R. Jones, A. Fraser, M.-A. Bray, D.J. Logan, K.L. Madden, V. Ljosa, C. Rueden, K.W. Eliceiri, A.E. Carpenter, Improved structure, function and compatibility for CellProfiler: modular high-throughput image analysis software, Bioinformatics 27 (2011) 1179–1180, https://doi.org/10.1093/bioinformatics/btr095.
[52] Z. Li, H. Wang, L.I. Zoungrana, A. James, L. Slotabec, S. Didik, M.K. Fatmi, M. Krause-Hauch, E.J. Lesnefsky, J. Li, Administration of metformin rescues age-related vulnerability to ischemic insults through mitochondrial energy metabolism, Biochem. Biophys. Res. Commun. 659 (2023) 46–53, https://doi.org/10.1016/j.bbrc.2023.04.004.
[53] G. Azhar, W. Gao, L. Liu, J.Y. Wei, Ischemia-reperfusion in the adult mouse heart influence of age, Exp. Gerontol. 34 (1999) 699–714, https://doi.org/10.1016/s0531-5565(99)00031-5.
[54] X. Chen, S. Ashraf, N. Ashraf, R. Harmancey, UCP3 (uncoupling protein 3) insufficiency exacerbates left ventricular diastolic dysfunction during angiotensin II-induced hypertension, J. Am. Heart Assoc. 10 (2021), e022556, https://doi.org/10.1161/JAHA.121.022556.
[55] E. Tzahor, K.D. Poss, Cardiac regeneration strategies: staying young at heart, Science 356 (2017) 1035–1039, https://doi.org/10.1126/science.aam5894.
[56] P.B. Garlick, M.J. Davies, D.J. Hearse, T.F. Slater, Direct detection of free radicals in the reperfused rat heart using electron spin resonance spectroscopy, Circ. Res. 61 (1987) 757–760, https://doi.org/10.1161/01.res.61.5.757.
[57] J.L. Zweier, P. Kuppusamy, R. Williams, B.K. Rayburn, D. Smith, M.L. Weisfeldt, J. T. Flaherty, Measurement and characterization of postischemic free radical generation in the isolated perfused heart, J. Biol. Chem. 264 (1989) 18890–18895.
[58] E.J. Lesnefsky, Q. Chen, S. Moghaddas, M.O. Hassan, B. Tandler, C.L. Hoppel, Blockade of electron transport during ischemia protects cardiac mitochondria, J. Biol. Chem. 279 (2004) 47961–47967, https://doi.org/10.1074/jbc.M409720200.
[59] T. Jr, Q. Cl, B. Md, Evidence for two sites of superoxide production by mitochondrial NADH-ubiquinone oxidoreductase (complex I), J. Biol. Chem. (2011) 286, https://doi.org/10.1074/jbc.M111.252502.
[60] E.L. Robb, A.R. Hall, T.A. Prime, S. Eaton, M. Szibor, C. Viscomi, A.M. James, M. P. Murphy, Control of mitochondrial superoxide production by reverse electron transport at complex I, J. Biol. Chem. 293 (2018) 9869–9879, https://doi.org/10.1074/jbc.RA118.003647.
[61] H.-S. Wong, P.-A. Monternier, M.D. Brand, S1QELs suppress mitochondrial superoxide/hydrogen peroxide production from site IQ without inhibiting reverse electron flow through Complex I, Free Radic. Biol. Med. 143 (2019) 545–559, https://doi.org/10.1016/j.freeradbiomed.2019.09.006.
[62] M.D. Brand, R.L.S. Goncalves, A.L. Orr, L. Vargas, A.A. Gerencser, M. Borch Jensen, Y.T. Wang, S. Melov, C.N. Turk, J.T. Matzen, V.J. Dardov, H.M. Petrassi, S. L. Meeusen, I.V. Perevoshchikova, H. Jasper, P.S. Brookes, E.K. Ainscow, Suppressors of superoxide-H2O2 production at site IQ of mitochondrial complex I protect against stem cell hyperplasia and ischemia-reperfusion injury, Cell Metabol. 24 (2016) 582–592, https://doi.org/10.1016/j.cmet.2016.08.012.

[63] S. Imai, A.L. Riley, R.M. Berne, Effect of ischemia on adenine nucleotides in cardiac and skeletal muscle, Circ. Res. 15 (1964) 443–450, https://doi.org/10.1161/01.res.15.5.443.
[64] M.-C.-I. Lee, M. Velayutham, T. Komatsu, R. Hille, J.L. Zweier, Measurement and characterization of superoxide generation from xanthine dehydrogenase: a redox-regulated pathway of radical generation in ischemic tissues, Biochemistry 53 (2014) 6615–6623, https://doi.org/10.1021/bi500582r.
[65] S.L. Thompson-Gorman, J.L. Zweier, Evaluation of the role of xanthine oxidase in myocardial reperfusion injury, J. Biol. Chem. 265 (1990) 6656–6663.
[66] R. Ascione, M. Caputo, W.J. Gomes, A.A. Lotto, A.J. Bryan, G.D. Angelini, M.-S. Suleiman, Myocardial injury in hypertrophic hearts of patients undergoing aortic valve surgery using cold or warm blood cardioplegia, Eur. J. Cardio. Thorac. Surg. 21 (2002) 440–446, https://doi.org/10.1016/s1010-7940(01)01168-x.
[67] A. Venturini, R. Ascione, H. Lin, E. Polesel, G.D. Angelini, M.-S. Suleiman, The importance of myocardial amino acids during ischemia and reperfusion in dilated left ventricle of patients with degenerative mitral valve disease, Mol. Cell. Biochem. 330 (2009) 63–70, https://doi.org/10.1007/s11010-009-0101-x.
[68] W.C. Stanley, G.D. Lopaschuk, J.L. Hall, J.G. McCormack, Regulation of myocardial carbohydrate metabolism under normal and ischaemic conditions, Poten. pharmacol. intervent. Cardiovasc Res. 33 (1997) 243–257, https://doi.org/10.1016/s0008-6363(96)00245-3.
[69] J.R. Ussher, W. Wang, M. Gandhi, W. Keung, V. Samokhvalov, T. Oka, C.S. Wagg, J.S. Jaswal, R.A. Harris, A.S. Clanachan, J.R.B. Dyck, G.D. Lopaschuk, Stimulation of glucose oxidation protects against acute myocardial infarction and reperfusion injury, Cardiovasc. Res. 94 (2012) 359–369, https://doi.org/10.1093/cvr/cvs129.
[70] T.N. Andrienko, P. Pasdois, G.C. Pereira, M.J. Ovens, A.P. Halestrap, The role of succinate and ROS in reperfusion injury - a critical appraisal, J. Mol. Cell. Cardiol. 110 (2017) 1–14, https://doi.org/10.1016/j.yjmcc.2017.06.016.
[71] C. Chinopoulos, Succinate in ischemia: where does it come from? Int. J. Biochem. Cell Biol. 115 (2019), 105580 https://doi.org/10.1016/j.biocel.2019.105580.
[72] J. Zhang, Y.T. Wang, J.H. Miller, M.M. Day, J.C. Munger, P.S. Brookes, Accumulation of succinate in cardiac ischemia primarily occurs via canonical Krebs cycle activity, Cell Rep. 23 (2018) 2617–2628, https://doi.org/10.1016/j.celrep.2018.04.104.
[73] V.R. Pell, A.-M. Spiroski, J. Mulvey, N. Burger, A.S.H. Costa, A. Logan, A. V. Gruszczyk, T. Rosa, A.M. James, C. Frezza, M.P. Murphy, T. Krieg, Ischemic preconditioning protects against cardiac ischemia reperfusion injury without affecting succinate accumulation or oxidation, J. Mol. Cell. Cardiol. 123 (2018) 88–91, https://doi.org/10.1016/j.yjmcc.2018.08.010.
[74] H. He, R.M. Mulhern, W.M. Oldham, W. Xiao, Y.-D. Lin, R. Liao, J. Loscalzo, L-2-Hydroxyglutarate protects against cardiac injury via metabolic remodeling, Circ. Res. 131 (2022) 562–579, https://doi.org/10.1161/CIRCRESAHA.122.321227.
[75] H.-G. Zimmer, H. Ibel, Ribose accelerates the repletion of the ATP pool during recovery from reversible ischemia of the rat myocardium, J. Mol. Cell. Cardiol. 16 (1984) 863–866, https://doi.org/10.1016/S0022-2828(84)80010-3.
[76] J.R. Neely, D. Feuvray, Metabolic products and myocardial ischemia, Am. J. Pathol. 102 (1981) 282–291.
[77] E. Liepinsh, M. Makrecka-Kuka, K. Volska, J. Kuka, E. Makarova, U. Antone, E. Sevostjanovs, R. Vilskersts, A. Strods, K. Tars, M. Dambrova, Long-chain acylcarnitines determine ischaemia/reperfusion-induced damage in heart mitochondria, Biochem. J. 473 (2016) 1191–1202, https://doi.org/10.1042/BCJ20160164.
[78] G.D. Lopaschuk, J.R. Ussher, C.D.L. Folmes, J.S. Jaswal, W.C. Stanley, Myocardial fatty acid metabolism in health and disease, Physiol. Rev. 90 (2010) 207–258, https://doi.org/10.1152/physrev.00015.2009.
[79] R.B. Jennings, K.A. Reimer, The cell biology of acute myocardial ischemia, Annu. Rev. Med. 42 (1991) 225–246, https://doi.org/10.1146/annurev.me.42.020191.001301.
[80] P. Korge, H.M. Honda, J.N. Weiss, Effects of fatty acids in isolated mitochondria: implications for ischemic injury and cardioprotection, Am. J. Physiol. Heart Circ. Physiol. 285 (2003) H259–H269, https://doi.org/10.1152/ajpheart.01028.2002.
[81] H. Tominaga, H. Katoh, K. Odagiri, Y. Takeuchi, H. Kawashima, M. Saotome, T. Urushida, H. Satoh, H. Hayashi, Different effects of palmitoyl-L-carnitine and palmitoyl-CoA on mitochondrial function in rat ventricular myocytes, Am. J. Physiol. Heart Circ. Physiol. 295 (2008) H105–H112, https://doi.org/10.1152/ajpheart.01307.2007.
[82] C. Metzsch, Q. Liao, S. Steen, L. Algotsson, Myocardial glycerol release, arrhythmias and hemodynamic instability during regional ischemia-reperfusion in an open chest pig model, Acta Anaesthesiol. Scand. 50 (2006) 99–107, https://doi.org/10.1111/j.1399-6576.2005.00877.x.
[83] P. Ferdinandy, T. Fazekas, E. Kádár, Effects of orotic acid on ischaemic/reperfused myocardial function and glycogen content in isolated working rat hearts, Pharmacol. Res. 37 (1998) 111–114, https://doi.org/10.1006/phrs.1997.0274.
[84] C. Aguer, B.D. Piccolo, O. Fiehn, S.H. Adams, M.-E. Harper, A novel amino acid and metabolomics signature in mice overexpressing muscle uncoupling protein 3, Faseb. J. 31 (2017) 814–827, https://doi.org/10.1096/fj.201600914R.
[85] L. Hardy, J.B. Clark, V.M. Darley-Usmar, D.R. Smith, D. Stone, Reoxygenation-dependent decrease in mitochondrial NADH:CoQ reductase (Complex I) activity in the hypoxic/reoxygenated rat heart, Biochem. J. 274 (Pt 1) (1991) 133–137, https://doi.org/10.1042/bj2740133.
[86] P.T. Kang, C.-L. Chen, P. Lin, L. Zhang, J.L. Zweier, Y.-R. Chen, Mitochondrial complex I in the post-ischemic heart: reperfusion-mediated oxidative injury and protein cysteine sulfonation, J. Mol. Cell. Cardiol. 121 (2018) 190–204, https://doi.org/10.1016/j.yjmcc.2018.07.244.
[87] G. Paradies, G. Petrosillo, M. Pistolese, N. Di Venosa, A. Federici, F.M. Ruggiero, Decrease in mitochondrial complex I activity in ischemic/reperfused rat heart: involvement of reactive oxygen species and cardiolipin, Circ. Res. 94 (2004) 53–59, https://doi.org/10.1161/01.RES.0000109416.56608.64.
[88] S.-B. Ong, S. Subrayan, S.Y. Lim, D.M. Yellon, S.M. Davidson, D.J. Hausenloy, Inhibiting mitochondrial fission protects the heart against ischemia/reperfusion injury, Circulation 121 (2010) 2012–2022, https://doi.org/10.1161/CIRCULATIONAHA.109.906610.
[89] K. D'Souza, C. Nzirorera, P.C. Kienesberger, Lipid metabolism and signaling in cardiac lipotoxicity, Biochim. Biophys. Acta 1861 (2016) 1513–1524, https://doi.org/10.1016/j.bbalip.2016.02.016.
[90] E. Silvestri, R. Senese, R. De Matteis, F. Cioffi, M. Moreno, A. Lanni, A. Gentile, R. A. Busiello, A.M. Salzano, A. Scaloni, P. de Lange, F. Goglia, A. Lombardi, Absence of uncoupling protein 3 at thermoneutrality influences brown adipose tissue mitochondrial functionality in mice, Faseb. J. 34 (2020) 15146–15163, https://doi.org/10.1096/fj.202000995R.